

Land consumption in cities: A comparative study across the globe

Jingliang Hu^a, Yuanyuan Wang^b, Hannes Taubenböck^{c,d}, Xiao Xiang Zhu^{a,b,*}

^a Data Science in Earth Observation (SiPEO), Technical University of Munich (TUM), 80333 Munich, Germany

^b Remote Sensing Technology Institute (IMF), German Aerospace Center (DLR), 82234 Wessling, Germany

^c Remote Sensing Data Center (DFD), German Aerospace Center (DLR), 82234 Wessling, Germany

^d Institute for Geography and Geology, University of Würzburg, 97074 Würzburg, Germany

ARTICLE INFO

Keywords:

Land consumption
Local climate zone (LCZ)
Population density
Sentinel-1
Sentinel-2
Topology enhanced ensemble classification
Urban land consumption
Urban morphology

ABSTRACT

Land consumption delineates how effectively we use our living space - whether wastefully in area or efficiently. As the United Nations (UN) projects 5.1 billion population will live in urban areas in 2030, it is crucial to measure, compare, and understand land consumption for our cities across the globe. Currently global approaches for land consumption analysis rely on settlement layers produced by remote sensing data and population data achieved by distributing census data over settlement layers. These layers, however, do not have sufficient spatial details to capture the intra-urban structural variability within a city. In this study, we develop a classification system that consistently produces accurate local climate zone (LCZ) maps at intra-urban scale for 40 cities using Sentinel data. We use the LCZ classes as proxies to disaggregate the global population grids (GHS-POP) to this intra-urban scale. With the refined data, we perform an intra-urban land consumption analysis for 40 cities across the globe. Our measurements shows that current per-city land consumption studies severely deviate from the intra-urban variability. We argue urban land consumption at global scale must proceed to an intra-urban resolution. In addition, our measurements also indicate that urban land consumption is differing immensely across the globe.

1. Introduction

1.1. Motivation

The United Nations (UN) reported that in 2018 already 55.3% of the world's population lived in urban areas (United Nations, 2018). This number is even estimated to increase to 60% by the year 2030. This means that for sustainable urban development, we have to weigh very well the land consumption. With the sustainable development goals (SDGs) set by the UN (United Nations, 2015b), the 11th goal is to make cities and human settlements inclusive, safe, resilient and sustainable. One specific indicator (SDG 11.3.1) for monitoring is described as "ratio of land consumption rate to population growth rate". According to the UN (United Nations Habitat, 2016), this indicator is particularly designed to monitor urban land consumption and thus, to measure the extent to which we use the space efficiently or wastefully. However, monitoring the intensity of usage or development of urban land at global scale in consistent manner remains a major challenge. Data generation is expensive both in finance and labour. Remote sensing technology, however, provides promising data sources to this challenge because it is

affordable and generally available at a global scale. Therefore, in this study we aim at studying urban land consumption of cities across the globe by using remote sensing data.

1.2. Conceptual foundation

The term 'urban land consumption' is generally defined as modified natural lands to man-made structures due to the living, social, and economic purposes of the urban residences (Boyce, 1963; d'Amour et al., 2017; Gerundo & Grimaldi, 2011). The term 'intensity of land consumption' is often an important quantitative measurement designed to reflect the status of the land consumption. Since one can study the urban land consumption from various disciplines, the intensity of land consumption has immense implications. From an economic perspective, (Kuang et al., 2020) defines it as the amount of urban land consumed per unit of gross domestic product (GDP); (Bimonte & Stabile, 2017) and (S. Wang, Cebula, et al., 2020) associate the term with income and housing price, respectively. Among urban temperature studies (He et al., 2019; Stokes & Seto, 2016; L. Xu et al., 2019; J. Yang et al., 2017; J. Yang, Wang, et al., 2020), the intensity of urban consumption is related to the

* Corresponding author at: Data Science in Earth Observation (SiPEO), Technical University of Munich (TUM), 80333 Munich, Germany.

E-mail address: xiaoxiang.zhu@dlr.de (X.X. Zhu).

building structure density that influences urban heat flow. From the scope of SDG (United Nations Habitat, 2016), the indicator focuses on the change of land consumption in time as the SDG indicator suggests by “ratio of land consumption rate to population growth rate”. From a demographic aspect, the intensity of land consumption relates to building structures which further influence the amount of population per unit of area (Freire et al., 2016; Glaeser, 2011). Moreover, (Martinez et al., 2007) found the population density an essential variable in the urban land consumption research with a case study in Puerto Rico. (Greklousis & Mountrakis, 2015) found a pro-linear relationship between the population and land consumption in the US. In our study, we use the indicator population density (the amount of population per spatial unit) as a measure of the intensity of land consumption. Our indicator reflects the efficiency of urban land usage from the demographic perspective.

Among the urban land consumption studies, many studies focus on a city (Lehnert et al., 2015; I. Stewart & Oke, 2009; Zhang et al., 2014) or a regional scale (Nicolau et al., 2019; Salvati et al., 2018; Y. Wang, Huang, et al., 2020; J. Yang et al., 2019; J. Yang, Zhan, et al., 2020). Few studies have approached urban land consumption on the global scale: (M. Melchiorri et al., 2018) analyzed the spatial dynamics of global urbanization from 1990 to 2015 by using the Global Human Settlement Layer (GHSL) (Pesaresi et al., 2013). They reported the planet became substantially more urbanized than what had been previously reported. Another study (M. Melchiorri et al., 2019) reported the urban land consumption of 10,000 cities by using the GHSL and analyzed the change of land use for these cities. (Taubenböck et al., 2019) analyzed 1692 cities from an urban morphological perspective by using the Global Urban Footprint (GUF) (Esch et al., 2017). They defined the extent of a city by a morphological urban area instead of an administrative boundary. Coupling with a population data, they found the Pearl River Delta is the largest urban agglomeration with the largest population on the planet. By far, thematically and structurally high resolution analyses are still limited to studies of a city or a regional scale. At the same time, global studies mostly rely on aggregate city so that their basic spatial unit is a city. They derived physical or statistical indicators per city for the analysis. This is because global settlement layers as the GUF (Esch et al., 2017) or the GHSL (Pesaresi et al., 2013) have a spatial resolution at the city scale. Intra-urban spatial information, however, are nonexistent on global scale.

Recently, new population layers on global scale have been introduced. Current population data are produced by distributing official census over built-up regions, such as gridded population of the world (GPW) (Doxsey-Whitfield et al., 2015) and global population grids (GHS-POP) (Freire et al., 2016). Additional data might also be used to regulate the spatial distribution. The WorldPop data considers land cover/land use information for distributing the population (Stevens et al., 2015). Census data, building footprint data and open street map data are applied in (X. Huang et al., 2019) to estimate the population distribution of the United States. In general, the spatial distribution of the global population data relies on the administrative areas of the census data and the spatial details of the settlement layers. Those settlement layers have coarse details, such as a binary built-up layer. All these factors result in limiting the spatial resolution of the population data at a city scale. Therefore, settlement layers of improved spatial and thematic resolutions at an intra-urban scale will promise a more accurate population distribution and urban land consumption study.

The available state-of-the-art global urban maps, GUF (Esch et al., 2017) and WSF (Marconcini et al., 2019), delineate the built-up area as a binary mask; and GHSL (Pesaresi et al., 2013), characterizes the urban area as a four-category thematic map considering the density of built-up areas (M. Melchiorri et al., 2019). Both products follow a classification scheme allowing to describe the spatial patterns of cities. With it, these data sets allow to compare the patterns of cities across space in a consistent manner. However, detailed morphological information within cities, such as the structural types of the settlements, is missing in these classifications. On the other hand, one recent scheme named Local

climate zones (LCZ) has often been applied for intra-urban morphological differentiation. The scheme aims at classifying urban areas in a consistent manner into 17 classes (I.D. Stewart & Oke, 2012). Although the LCZ classification scheme was originally designed for urban climatic studies (I.D. Stewart et al., 2014; I.D. Stewart & Oke, 2012), it essentially classifies the urban area by morphological criteria, mainly including the compactness, the structural shape, and the heights of settlements, as well as the land surface material. Indirectly, those morphological parameters also allow for deriving land use information to a certain degree (B. Bechtel, Pesaresi, et al., 2016; Perera & Emmanuel, 2018; Sapena et al., 2021; X.X. Zhu et al., 2020). Thus, in comparison to the current state-of-the-art global urban mappings, the LCZ scheme can provide intra-urban morphological information to account for the morphological variance within the settlement landscape. With it and in combination with population data, the analysis of urban land consumption allows for an intra-urban spatial scale.

Based on the conceptual foundation, in this study, we aim at studying and comparing urban land consumption in various cities across the globe at an intra-urban spatial scale to account for the variability within cities. We aim to show the extent to which urban living space is used effectively or ineffectively. In particular, we want to show that indicators that are usually generated at the city scale are susceptible to deviating mean values due to the high variability of land consumption intensity within cities.

1.3. Contribution of this article

In this study we investigate urban land consumption by associating demographic information to intra-urban knowledge on structural variability by the LCZs. The contributions of this article are three fold: **First**, in this paper we analyze urban land consumption at global scale, but compared to existing literature we increase the spatial resolution from city- to an intra-urban scale. We argue that monitoring the urban land consumption or urban sustainable development at global scale must proceed to an intra-urban resolution, as we find our estimated city-scale urban land consumption indicators severely deviate from the intra-urban variabilities. **Second**, this paper develops a novel semi-supervised data-topology based classification system which fuses freely-accessible Sentinel-1 and Sentinel-2 data. The developed system is capable of providing urban morphological maps for cities around the globe with intra-urban spatial details in consistent and thus comparable manner. Only with this, we believe that a cross-city comparison is permissible. In this study we apply it for 40 cities around the globe. **Third**, compared to existing population data that distribute demographic census data over settlement layers, this paper improves the granularity of the settlement layers to 11 types of urban morphological classes for the population distribution. With it, we integrate beyond morphological details also the functionalities of these classes. The refined population grid has a reasonable distribution at the intra-urban scale and with unprecedented 10 m spatial resolution.

The remainder of this paper is as follows. Section 2 introduces the study areas, the data, and the methodology. In section 3, we present the evaluation of the developed classification system, demonstrate the spatially refined population data, and analyze land consumption. Section 4 discusses the outcomes of our studies. And section 5 concludes this paper.

2. Data and method

2.1. Study area

We base our selection of study areas on five rules: First, the selection of cities has a global distribution, i.e. we select cities from all continents. Second, the selected cities are from different cultural regions, i.e. even within continents we select cities that are of different cultural regions. Third, the cities are of different status in terms of development and

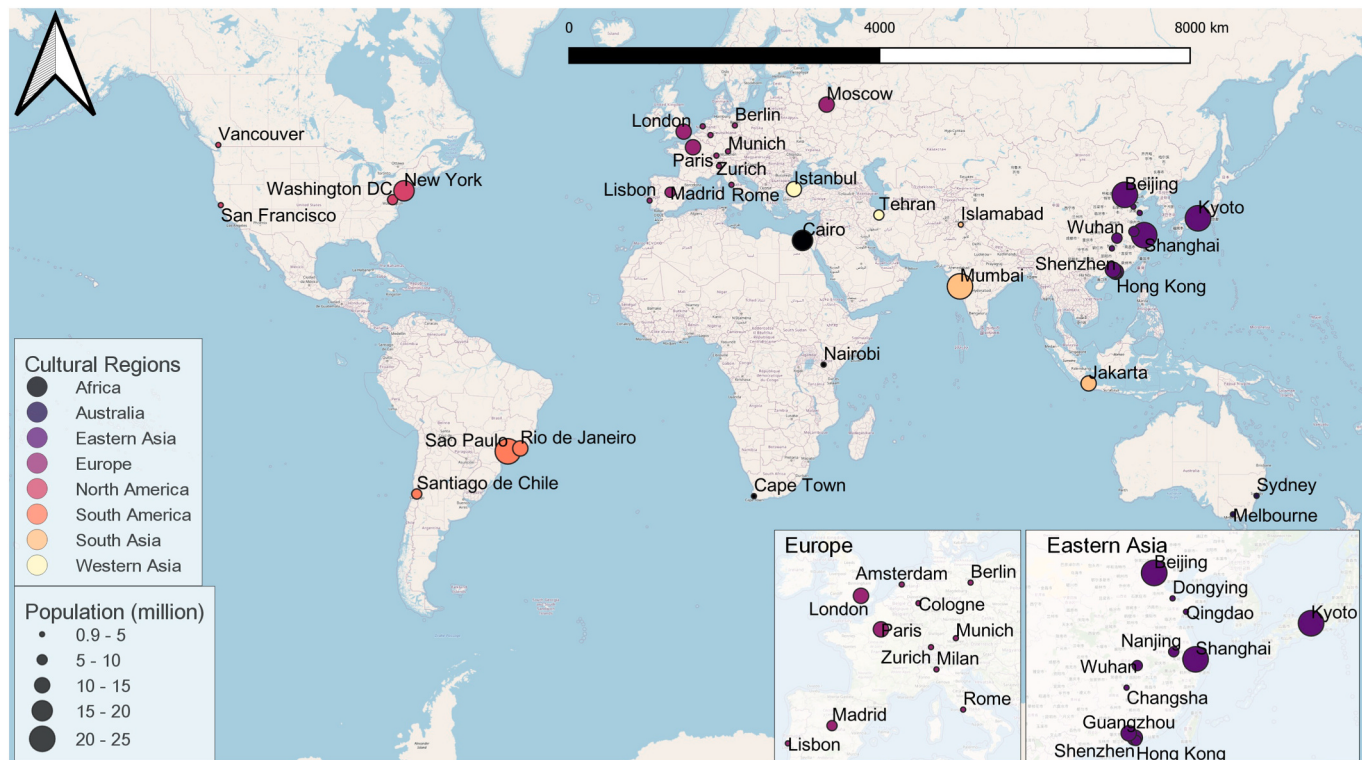


Fig. 1. The geographic locations of the 40 sample cities. The size and colour reflect the population and cultural region of the corresponding city.

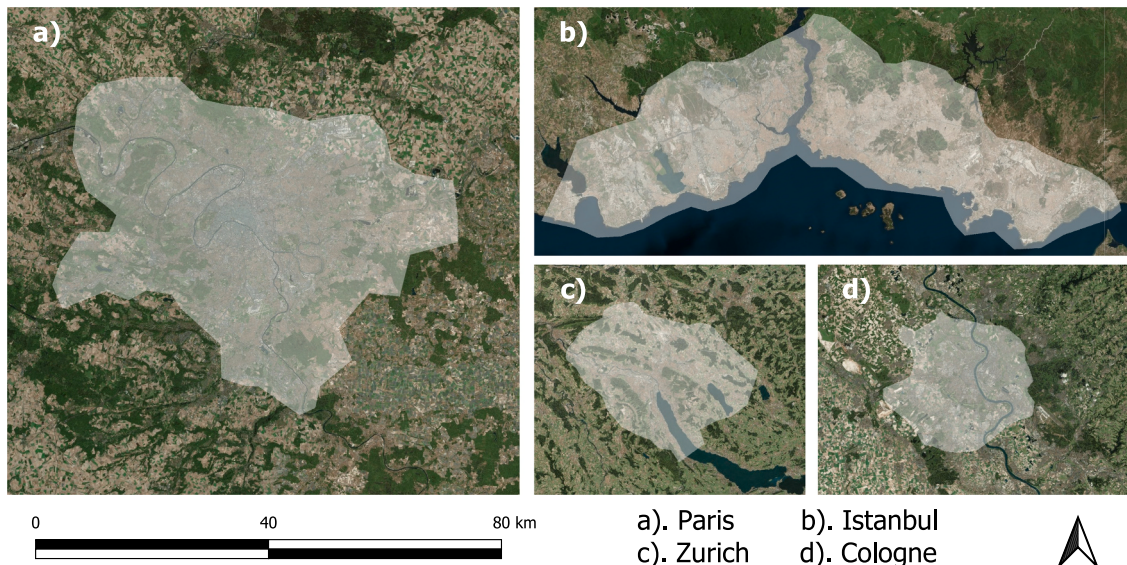


Fig. 2. The cities of Paris, Istanbul, Zurich, and Cologne are shown in the same map scale where the highlighted areas indicate MUA urban extents (Taubenböck et al., 2019).

economy. Fourth, these cities are large cities where urban morphology are very complex and challenging for the algorithm development. As large cities, they feature large population as well. Fifth, from a pragmatic point of view, we selected cities where LCZ reference data are available and accessible (X.X. Zhu et al., 2020). Based on these general rules, we selected 40 major cities. As shown in Fig. 1, the selected cities cover nine cultural regions, namely Australia, East Asia, South-east Asia, the Indian subcontinent, the Middle East, Europe, Africa, North America, and South America. Moreover, the selection includes economically less-developed cities, such as Islamabad, and very-developed cities, such

as London. The selected cities all have comparably large population, which in total are according to UN statistic (United Nations, 2015a; United Nations, 2016) home to about 343 million inhabitants in the year of 2015.

For a permissible comparative study of cities, comparable spatial units, i.e. spatial extents of cities, need to be defined. The administrative boundary of a city often does not reflect the physical extent of the city. An extent of fixed radius, however, is also not meaningful due to large variety in size and shape of our sampled cities. For example, as shown in Fig. 2, the sizes and shapes of Paris, Istanbul, Zurich, and Cologne have

huge differences. Against this background we apply morphological urban areas (MUA) introduced by (Taubenböck et al., 2019). The MUA delineates the extent of a city from the urban landscape along a decreasing gradient of settlement density. Based on quantitative measure, the MUAs are consistent among cities and thus are permissible spatial extents for meaningful comparative studies. The highlighted areas in Fig. 2 demonstrate the MUA extents of the cities.

2.2. Data sets

We base this study on remotely sensed as well as auxillary data. For the generation of the LCZ classification we rely on three data sources: 1) **Sentinel-1 data**, 2) **Sentinel-2 data**, and 3) **an LCZ reference data**. For the population information we use 4) **the GHS-POP**.

- 1) **Sentinel-1 data** used in this paper are level-1 VV-VH dual-Pol single look complex (SLC) products. The data are prepared as an analysis-ready data of 10 m ground sampling distance via a group of pre-processing steps using the ESA SNAP toolbox. The detailed procedure of the preprocessing is introduced in Appendix A.

After the preprocessing, feature extraction is carried out on the analysis-ready data for the classification purpose. It is designed to derive features representing polarimetric information, local neighborhood information, and spatial information. The features related to polarimetric information are the intensity of VV, the intensity of VH, the coherence between VV and VH, and the intensity ratio of VV and VH. The intensity features are converted into decibel (dB). The local neighborhood information includes the mean and the standard deviation of an 11-by-11-pixel local area for each of the four polarimetric features. The spatial information is derived by the morphological profile (Benediktsson et al., 2003; Fauvel et al., 2008), with radius of 1, 2, and 3 pixels, for each of the four polarimetric features. The feature extraction results in 36 features in total.

- 2) **Sentinel-2 data** are preprocessed on Google Earth Engine (GEE) for eliminating clouds (Gorelick et al., 2017; Schmitt et al., 2019). Afterwards, feature extraction is carried out on the Sentinel-2 analysis-ready data which also has a ground sampling distance of 10 m for the classification purpose. The principal components of the data that hold 99% of the total spectrum information are derived to represent the spectral information. The morphological profile is utilized to derive the spatial information on each of the principal component, with radius of 1, 2, and 3 pixels. Thus, the number of extracted S2 features varies from city to city depending on the numbers of principal components.
- 3) **The LCZ reference data** used in this paper is from the So2Sat LCZ42 (X.X. Zhu et al., 2020). These have been annotated by a group of 15 experts who followed a labeling protocol that maximizes its consistency, completeness, and correctness, meanwhile minimizes inevitable human error (X.X. Zhu et al., 2020). For each of the 40 cities, the reference data is formatted as a raster image with a ground sampling distance of 100 m. It is important to mention that, instead of the original 17 classes of LCZ, this paper aims to classify a modified version of LCZs with 11 classes. The main reason of modifying the LCZ scheme is that there is no access to global scale data that provides reliable, accurate and complete building height information for urban areas. The 17 classes of the original LCZs describe four properties of urban land: compactness, structural shape, height of settlements and the land surface. Since the satellite data used in our study have no information on height, we modify the LCZ classification scheme by merging the LCZs of ‘compact high rise’, ‘compact middle rise’, and ‘compact low rise’ as *compact structures*, and the ‘open high rise’, ‘open middle rise’, and ‘open low rise’ as *open structures*. By cross check with satellite images, the large low rise class very often consists of warehouses or factories located in

industrial areas so that we merge the classes of ‘large low rise’ with ‘heavy industry’ to an *industrial area*. The sparsely built-up is ignored because it frequently locates in scattered tree area or low plant area. Therefore, we come up with a modified version of LCZ with 11 classes.

- 4) **The population data** used in this paper is a world-wide grid of the population for 2015, namely GHS-POP (Schiavina et al., 2019). In the grid, each cell has a ground sampling distance of 250 m and provides the number of people. The data is achieved by disaggregating administrative census data over a global built-up layer, the Global Human Settlement Layer (GHSL) (Pesaresi et al., 2013).

2.3. Method

The goal of this study is to analyze land consumption at the intra-urban scale. To meet the goal, we first develop a classification system that fuses the Sentinel-1 and Sentinel-2 data and classifies the fused data into LCZ maps. Two main modules of the classification system are a semi-supervised data fusion and a data topology based ensemble classification. Details of the two modules are introduced in Section 2.3.1 and 2.3.2, respectively. To reflect the accuracy of the produced LCZ maps, a sophisticated strategy is designed for a systematic evaluation, which is introduced in Section 2.3.3. Secondly, we use the LCZ classification maps to refine population data. We do so by redistributing the population into possible residential areas. Details are introduced in Section 2.3.4. At last, an unsupervised clustering module is developed to identify types of urban morphological formation which enables analyzing the correlation between land consumption and morphological types of cities. This approach is detailed in Section 2.3.5.

2.3.1. Semi-supervised data fusion

The developed classification system fuses Sentinel-1 and Sentinel-2 data, i.e. optical and radar data, via a semi-supervised strategy. In previous studies, researches have investigated optical data (B. Bechtel, 2011; Danylo et al., 2016; Y. Xu et al., 2017), digital surface models (DSM) (B. Bechtel & Daneke, 2012; Z. Xu et al., 2018), geographical information system (GIS) data (Gál et al., 2015; Geletič & Lehnert, 2016; Lelovics et al., 2014), Interferometric Synthetic Aperture Radar (InSAR) (B. Bechtel & Daneke, 2012), and polarimetric synthetic aperture radar (PolSAR) data (B. Bechtel, See, et al., 2016; J. Hu et al., 2018) for the classification task. Commonly, optical data have been used for their easy access and good performance. However, these data are limited by weather conditions. Beside being independent from weather conditions, PolSAR data are beneficial by providing spatial information and back scatterings of built-ups. To join the merits of both data sources, we apply Sentinel-1 and Sentinel-2 data for mapping LCZ. The reasons are: (1) the two data sources, the multispectral information and the radar back scattering, provide complementary physical information; (2) both data sources have global coverage and are freely accessible; (3) optical data have a good performance on LCZ classification (B. Bechtel, 2011; Qiu et al., 2019; Y. Xu et al., 2017), but data availability depends on weather conditions, while Sentinel-1 data is available independent to weather conditions; (4) it has been proven that spatial information and polarimetric information of SAR data benefit LCZ classification (B. Bechtel, See, et al., 2016; J. Hu, Hong, Zhu, et al., 2019).

Data annotations are of great importance for machine learning algorithms (Reichstein et al., 2019; X.X. Zhu et al., 2017). Yet annotating land cover/use information in remote sensing is very expensive in cost and labour. Thus, an algorithm that takes maximum advantage of information in data annotations is highly welcomed. For the combined usage of Sentinel-1 and Sentinel-2 data, we follow a semi-supervised data fusion strategy (J. Hu, Hong, Zhu, et al., 2019; Tuia et al., 2014; C. Wang & Mahadevan, 2009). This strategy propagates the information of annotated data into un-annotated data via the similarity measure between them. It is able to amplify the information in annotations which is beneficial in remote sensing. Therefore, the semi-supervised strategy

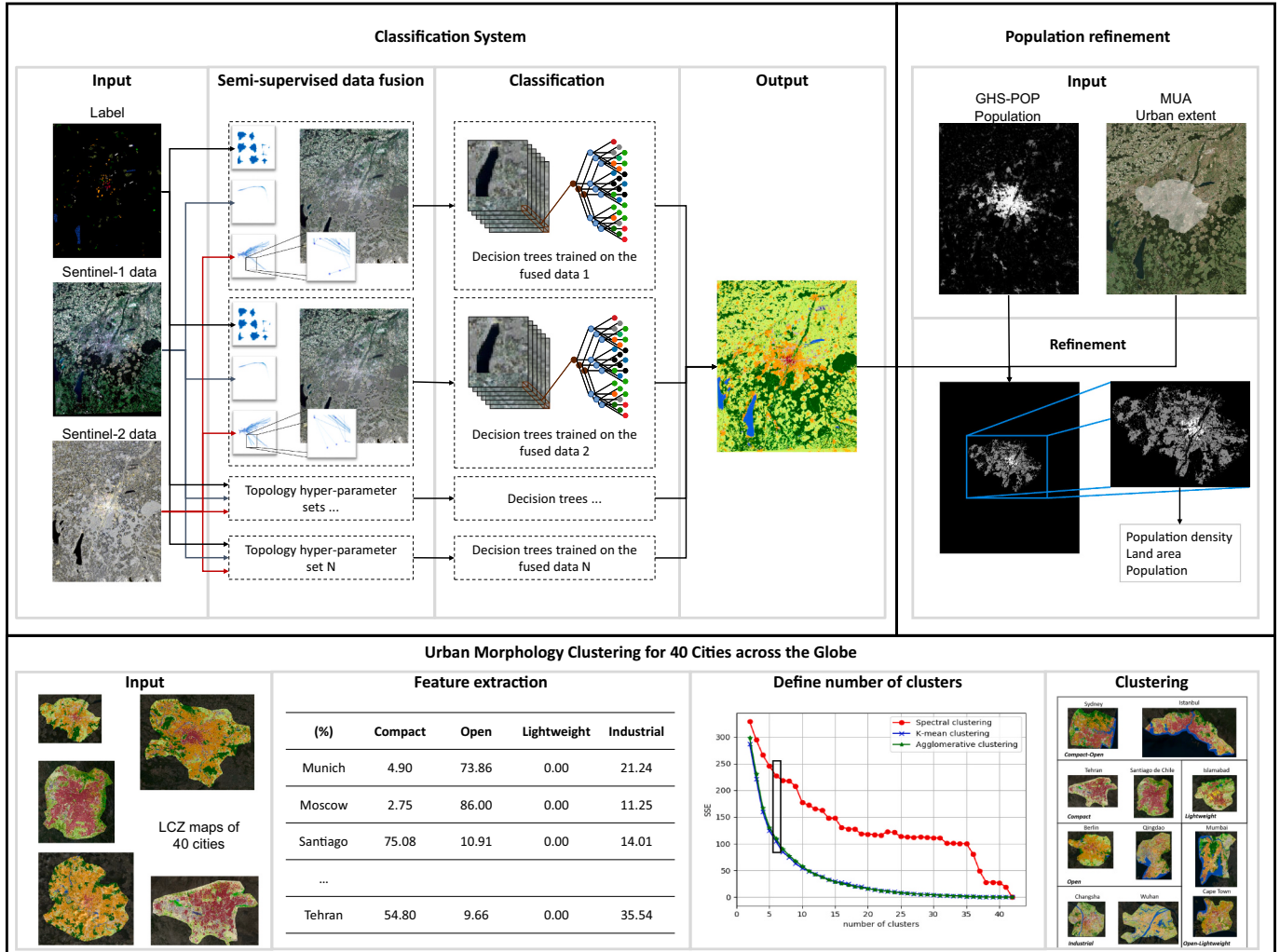


Fig. 3. The methodological workflow of classification, population refinement, and urban clustering. The classification takes Sentinel-1 data, Sentinel-2 data, and LCZ reference data as inputs and produces LCZ maps. The population refinement takes the produced LCZ map, GHS-POP data, and the MUA urban extent to improve the spatial details of the population data. The urban clustering takes 40 LCZ maps as inputs and identifies city types in terms of morphological formations.

is utilized in our data fusion module.

The semi-supervised fusion algorithm aims to map Sentinel-1 and Sentinel-2 data into a latent space where (I) the data of the same class locate close to each other, and (II) the topological structure of individual data source is preserved. As shown in the semi-supervised data fusion of Fig. 3, the class-wise relation, the property (I) of the latent space, is derived from reference data and represented as a graph. With a topological data analysis tool (Singh et al., 2007; Li et al., 2015), the data structures of the two data sources are presented as two graphs, which stands for the second property of the latent space. Those three graphs can be organized and formulated by using a joint similarity matrix. With the joint similarity matrix, a general eigenvalue problem is formulated and a mapping function for each of the data sources can be optimized. Therefore, the two mapping functions act as the bridges that link the two data sources to the latent space, respectively. More mathematical background of the semi-supervised data fusion algorithm is introduced in Appendix B.

2.3.2. Topology enhanced ensemble classification

It has been shown that a group of classification algorithms (Danylo et al., 2016; Geletić & Lehnert, 2016; Lelovics et al., 2014; Z. Xu et al., 2018) is beneficial for producing LCZ maps for a city by a classifier trained with data of that city. Another group of algorithms attempt to train a classifier and produce LCZ maps for cities where reference data

are not available (Demuzere et al., 2019; Kaloustian et al., 2017; Tong et al., 2020; Yokoya et al., 2017; Zheng et al., 2020). Due to local specific algorithms of the first group result in better classification accuracy compared to the second group. With this background, we followed the strategy of the first group and produced LCZ maps for selected 40 cities where LCZ labels are available.

Random forest is chosen as classifier for our classification system, since it is a state-of-the-art, non-parametric, and time efficient classifier that is widely used in global scale classification tasks (C. Li et al., 2017) and local climate zone classification tasks (B. Bechtel et al., 2015; Demuzere et al., 2019; Yokoya et al., 2017). The random forest trains its decision trees with random subset of features and random subset of training samples. It results in different decision trees predicting different labels for an instance. This configuration creates a diversity that empowers random forest the most. The diversity makes random forest statistically following the *Law of Large Numbers* so that it has a robust performance, avoids overfitting, and meanwhile preserves the computational efficiency (Breiman, 2001; Elghazel et al., 2011; Rainforth & Wood, 2015).

In the proposed classification system, there is a practical issue of hyper parameter optimization while deriving topological structures. No matter which method is chosen to obtain topological structures of Sentinel-1 and Sentinel-2 data, one would inevitably be confronted with the optimization of hyper-parameter. To handle this practical issue, a

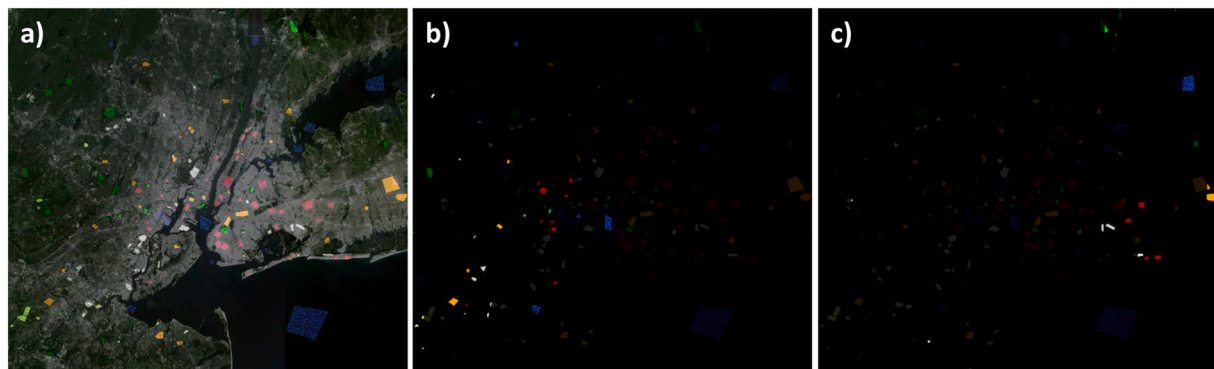


Fig. 4. The reference data are equally separated into ten non-overlapping subsets from west to east for each city. This figure shows the procedure by the example of New York. In this figure, the three images are: a) the reference data overlapped with the RGB imagery; b) the reference data with the first subset highlighted; c) the reference data with the tenth subset highlighted.

study (Tuia et al., 2014) set the hyper-parameter manually based on their empirical experiences. Another study (J. Hu, Hong, Zhu, et al., 2019) reported that no statistically significant optimal solution can be found. In this paper, the authors find that varying values of the hyper-parameter leads to topological structures of regional differences. Inspired by the *Law of Large Numbers* concept in random forest classifier, this paper proposes a topology enhanced ensemble classification scheme. It fuses the two data sets with a set of hyper-parameter. For each fused data set, a group of decision trees are trained. Therefore, in the prediction phase, the ensemble of decision trees includes diversities of three aspects: different topological structures, random subset of features, and random subset of training samples.

2.3.3. Classification evaluation strategy

To evaluate the performance of the proposed classification system, we design a sophisticated evaluation strategy that is able to avoid overestimation of classification accuracy caused by overfitting and that provides an uncertain range of accuracy in a statistical robust manner.

For evaluating an algorithm, the spatially random selection of training data from the ground reference that often appears in literature will make the training and the testing samples strictly follow the same distribution. Such selection of training data results in the trained algorithm overfitting the test data. In consequence the resulting accuracy would overestimate the performance of the trained algorithm (Hänsch et al., 2017). To avoid the overestimation, we separate the ground reference into blocks for training and testing.

The fractions of reference data used for training and testing would also have an impact on the accuracy assessment. In remote sensing applications, the training data normally cover an extremely small fraction of the whole study area. As an example in subplot a) of Fig. 4, this fraction can be observed by comparing the coverage of reference data to the extent of New York. However, in machine learning evaluation, training data often occupy 90% of reference data and the remaining 10% are used as testing data. The amount of training data is nine times larger than the testing data, which is not realistic in remote sensing. Thus, in our evaluation, instead of only taking 90% of reference data as training data, we take 10%, 50%, and 90% of the reference data as training data for three sets of evaluations, respectively. To achieve this setting, reference data are equally separated into ten block-wise subsets, as shown in Fig. 4. In our configuration, instead of one accuracy, the three settings will provide a range of accuracies indicating possible performance of an algorithm with respect to the amount of training samples used. For each of the three settings, a 10-fold cross validation is performed to achieve a mean classification accuracy which is a statistical robust indicator.

2.3.4. Population refinement and population density

Current high resolution population data are generally achieved by spatially distributing official census data at administrative levels over settlement areas detected from remote sensing data. However, this is in large area applications predominantly done regardless of the functionality of the settlement structures. Therefore, the disaggregation procedure might lead to people assigned to industrial sites and thus might lead to a skewed inaccurate calculation of the population density at intra-urban scale. As we associate population to urban land for analyzing urban land consumption in this paper, the population density is applied as an important quantitative indicator for the analysis. To avoid the miscalculation of population density, we refine the population data using the morphologic and functional knowledge of our classified LCZ maps. Although the local climate zones was originally designed for the study of land surface temperatures, the classification scheme essentially describes the structures of local urban neighborhoods in terms of the compactness, the shape, the height, and the covering materials of the settlements. And these characteristics of local urban neighborhoods reflect the population distribution within a city. We rely on these data to redistribute the given population data from GHS-POP. For the refinement, we assume, (1) people do not live in industrial structures, and (2) the population density of compact, open, and lightweight structures differ, due to the varying available living spaces within these morphological structures.

To accomplish the refinement, the population over industrial structures in the GHS-POP data need to be redistributed to the other three structures. The ratios of population that reside in the other three structures are calculated based on the produced LCZ map and the population data. In detail, an LCZ map is presented as a grid \mathcal{L} . \mathcal{L}_j^i presents a cell in the grid where $i \in \{C, O, L\}$ stands for compact, open, lightweight, and industrial structures, and $j \in \{1, 2, \dots, n\}$ stands for the j th cell. The population data is presented as a grid \mathcal{P} and \mathcal{P}_j^i geographically corresponds to \mathcal{L}_j^i . Therefore, the ratios of population that reside in compact, open, and lightweight structures are calculated according to (1).

$$R_i = \frac{\sum_j \mathcal{P}_j^i}{\sum_i \sum_j \mathcal{P}_j^i}, i \in \{C, O, L\} \quad (1)$$

Then, the calculated ratios guide the redistribution of the current population to achieve the refined population grid $\tilde{\mathcal{P}}$.

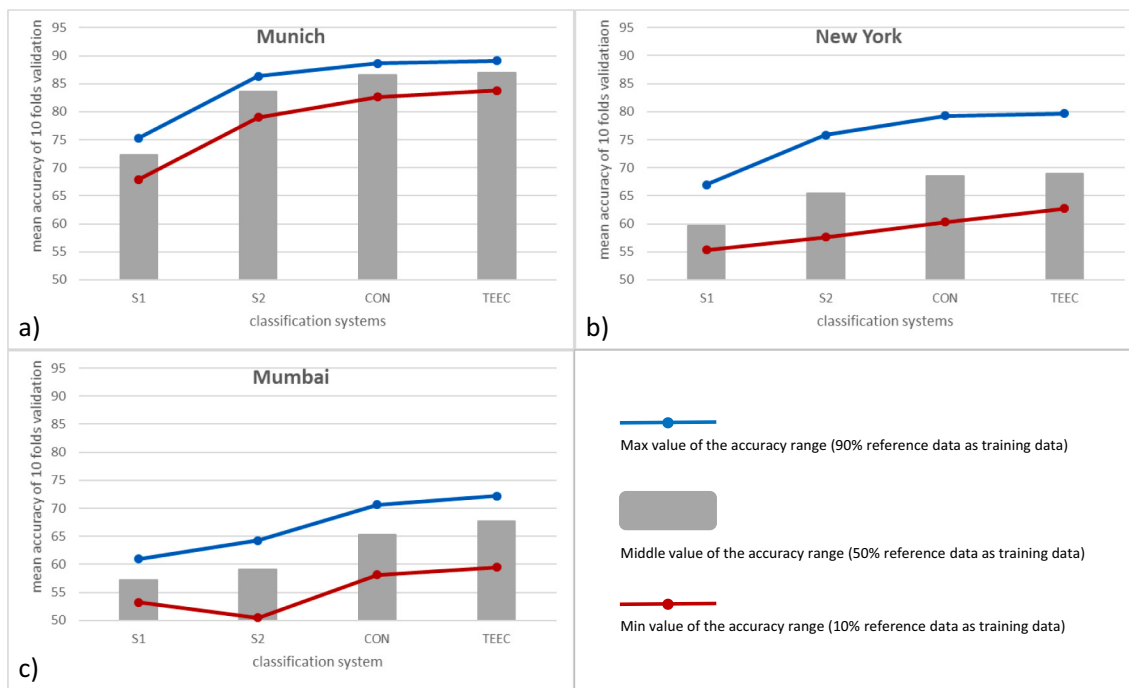


Fig. 5. Evaluation of four classification systems, S1, S2, CON, and TEEC. The x-axis indicates the respective classification system. The y-axis depicts the mean overall accuracy of the 10-folds cross-validation evaluation. The three subplots a), b) and c) represent the evaluation over Munich, New York, and Mumbai. The blue curve shows the accuracies that are achieved by using 90% reference data as training data, which can be regarded as the upper bound of the accuracy. The red curve shows the accuracy produced by using 10% reference data as training data, which can be regarded as the lower bound of each method. And the grey bar shows the accuracy produced by using 50% reference data as training data as a median value between boundaries. (For interpretation of the references to colour in this figure legend, the reader is referred to the web version of this article.)

$$\tilde{\mathcal{P}}_j^i = \begin{cases} \frac{\sum_{i,j} \mathcal{P}_j^i \times R_i}{n^i} & i \in \{C, O, L\}, n^i : \text{the cell number of the } i \text{ structure} \\ 0 & i = I \end{cases} \quad (2)$$

For our assessment of land consumption, we rely on the population density that is calculated based on our refined population data. We apply our analysis on land consumption at two spatial scales - on city scale and on intra-urban scale. On the city scale we calculate the 'land area' as the sum of all settlement areas from the compact, open and lightweight structures, i.e. from areas where we assume people live. The population is calculated as the total population of a city which refers to the input population data and the applied MUA. The population density equals the total population divided by the possible living areas. Based on the fusion of both products, we provide these three indicators to reflect land consumption. On the intra-urban scale, these three indicators are calculated for compact, open, and lightweight urban blocks. This scale allows for an intra-urban analysis, that would not be possible by using only original population data.

2.3.5. Clustering of cities based on their morphological formations

For our urban geographic analysis, we want to identify morphological types that are similar in their built configuration. For the clustering procedure, we use features from the LCZ maps that represent the morphological formation of a city. We calculate the spatial proportions of the four urban morphological structures, compact, open, light, and industrial structure in the built-up areas. With this feature representation, it becomes possible that cities with large differences in size and shape can be recognized as the same type based on similar morphological formations.

We apply clustering to find urban morphological groups. Two critical issues are: (1) choosing a clustering algorithm and (2) defining the

number of clusters. For choosing an algorithm, there exist two groups of algorithms that are divided by strategies of deciding the number of clusters. The first group of algorithms has the number of clusters as an input parameter which users must know in advance, such as K-mean clustering (Arthur & Vassilvitskii, 2007), spectral clustering (Ng et al., 2002; Von Luxburg, 2007), and agglomerating clustering (Frigui & Krishnapuram, 1997). The second group of algorithms detects the number of clusters by physical or statistical variables in an algorithm whose values have to be given in advance. Instead of explicitly giving the number of clusters, these thresholds having physical or statistical meanings indirectly decide the number of clusters. Such algorithms include e.g. DBSCAN (Ester et al., 1996), mean shift (Comaniciu & Meer, 2002), modified spectral clustering (Zelnik-Manor & Perona, 2005), or topological persistence based clustering (Chazal et al., 2013). For the sake of simplicity and robustness, we choose K-means. For the second issue, defining the number of clusters, the error sum of squares (SSE) is utilized as a quantitative indicator. SSE is the sum of squared error between each data record and the mean cluster center.

$$SSE = \sum_{i=1}^n \left(\mathbf{C}_i - \tilde{\mathbf{C}}_i \right)^2 \quad (3)$$

where n is the number of data records, \mathbf{C}_i is a feature vector representing the i^{th} data record, and $\tilde{\mathbf{C}}_i$ is the center of the cluster that the i^{th} record belongs. With SSE, the rule of elbow is a frequent practice of deciding the number of clusters (Jain et al., 1999). It chooses the value whose increase brings a small reduction of the SSE and those non-relevant groups. To decide the number of clusters, we apply K-means clustering, spectral clustering, and agglomerating clustering to cluster sample cities with the number of clusters ranging from 2 to the maximal possible value. Therefore, an SSE curve in terms of the number of clusters can be plotted. By considering the rule of elbow for all three algorithms, the number of clusters can be chosen.

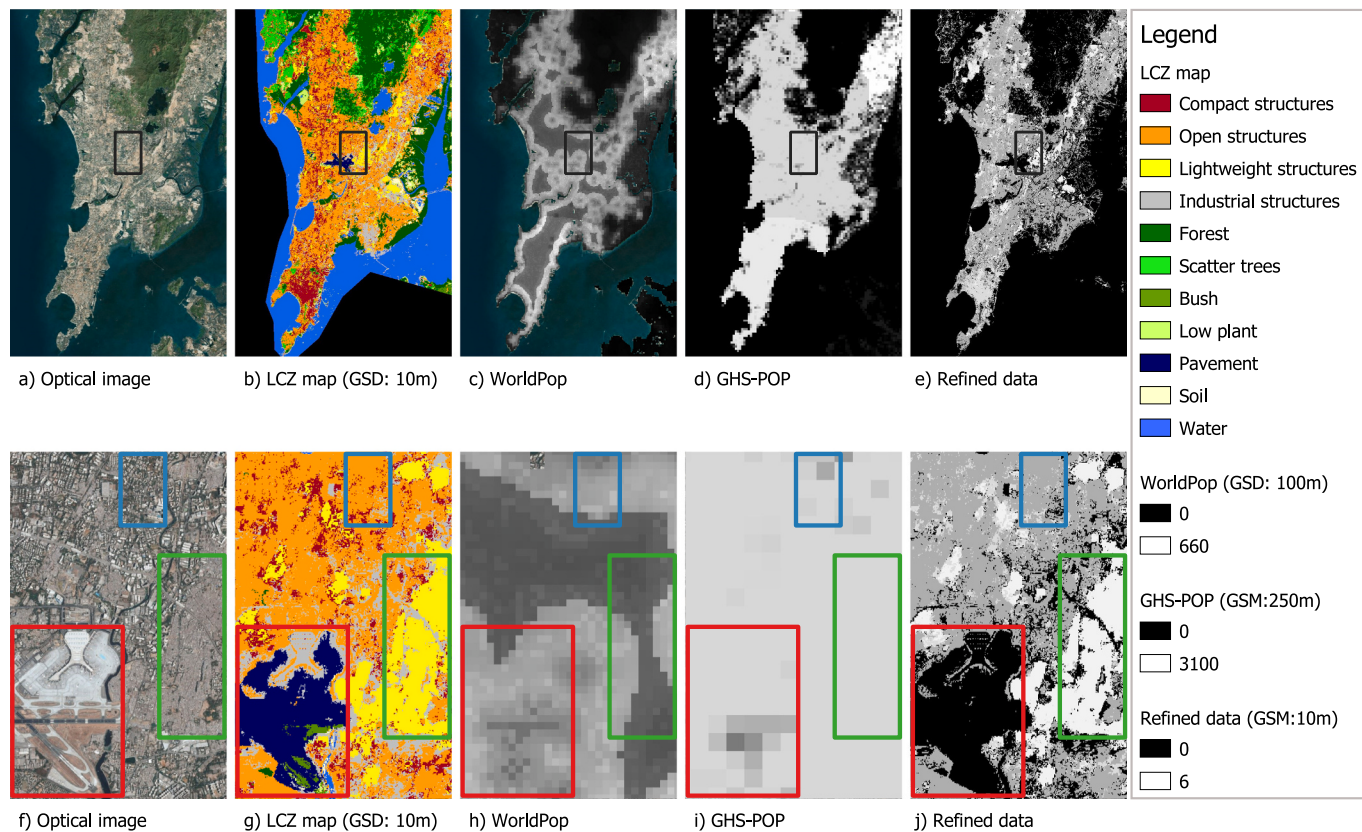


Fig. 6. This figure demonstrates the LCZ map, the WorldPop population data (Tatem, 2017), the GHS-POP population data (Schiavina et al., 2019), and our refined population data for the city of Mumbai. The images in the first row show: a) the optical image, b) the LCZ map, c) the WorldPop data, d) the GHS-POP data, and e) our refined data of Mumbai. In the second row, we detail the airport district in Mumbai to demonstrate the spatial refinement based on our LCZ classification against the state of the art population data. In the zoomed images, the blue, red, and green rectangles indicate an open area, an airport, and a compact area, respectively. GSD stands for ground sampling distance. (For interpretation of the references to colour in this figure legend, the reader is referred to the web version of this article.)

3. Results and analysis

In this section, first, we evaluate the performance of the proposed classification procedure and population refinement. Then, we present and compare the land consumption of the sampled 40 cities at city scale and the intra-urban scale. At last, we summarize our analysis.

3.1. Evaluation

3.1.1. Evaluation of the LCZ classification

Following the strategy introduced in Section 2.3.3, we present the evaluation of the proposed classification system for three morphologically different exemplary cities: Munich, New York and Mumbai.

We applied three other classification systems for comparisons. They are: (1) Sentinel-1 data with random forest (S1); (2) Sentinel-2 data with random forest (S2); (3) the concatenation of Sentinel-1 and Sentinel-2 data with random forest (CON). The three classification systems are chosen for comparison because such systems have appeared on large scale classification tasks in literature (Ban et al., 2015; Demuzere et al., 2019; Esch et al., 2017; C. Li et al., 2017; Lisini et al., 2017; Yokoya et al., 2017; Z. Zhu et al., 2012). The proposed classification system is indicated by topology enhanced ensemble classification (TEEC) in the evaluation 5.

Fig. 5 demonstrates the ranges of the achieved mean overall accuracy by the 10-fold validation. The range shows accuracies achieved by using different amounts of reference data as training data, namely 10%, 50%, and 90% of the reference data. According to Fig. 5, the proposed classification system outperforms the other systems in terms of the mean overall accuracy, under all scenarios of different training sets and cities.

For the city of Munich, the proposed classification system reaches a mean overall accuracy from 83.8% to 89.1%. For the city of Mumbai which has a complex urban environment, our system has an accuracy from 59.4% to 72.2%. The accuracy for the city of New York ranges from 62.8% to 79.7%. With the sophisticated evaluation strategy, we conclude the proposed classification system allows to produce with respect to commonly used algorithms highly accurate and consistent LCZ classifications for our 40 cities.

3.1.2. Evaluation of the population refinement

For the evaluation of the spatial refinement of population data, we present the results by the example of Mumbai. As high resolution ground truth population data are nonexistent, we aim to provide a qualitative analysis for our refinement of the population. As shown in Fig. 6, it seems very plausible that our refinement of the population improves the global data due to the spatial detail in our LCZ classification. For example, the blue, red, and green boxes outline an open area, an airport, and a compact area, respectively. In GHS-POP data, the population density are the same for the three areas. In WorldPop data, the population that reside in the airport and open area is larger than the population in lightweight area. Both cases seem to be very unrealistic. In our refined data, the re-distribution of population appears more reasonable as in the airport we do not have population disaggregated.

3.2. Land consumption of cities across the globe

Based on the results presented above, we now analyze and compare land consumption in and across our selected 40 cities. The term land consumption describing the lands that have been modified from its

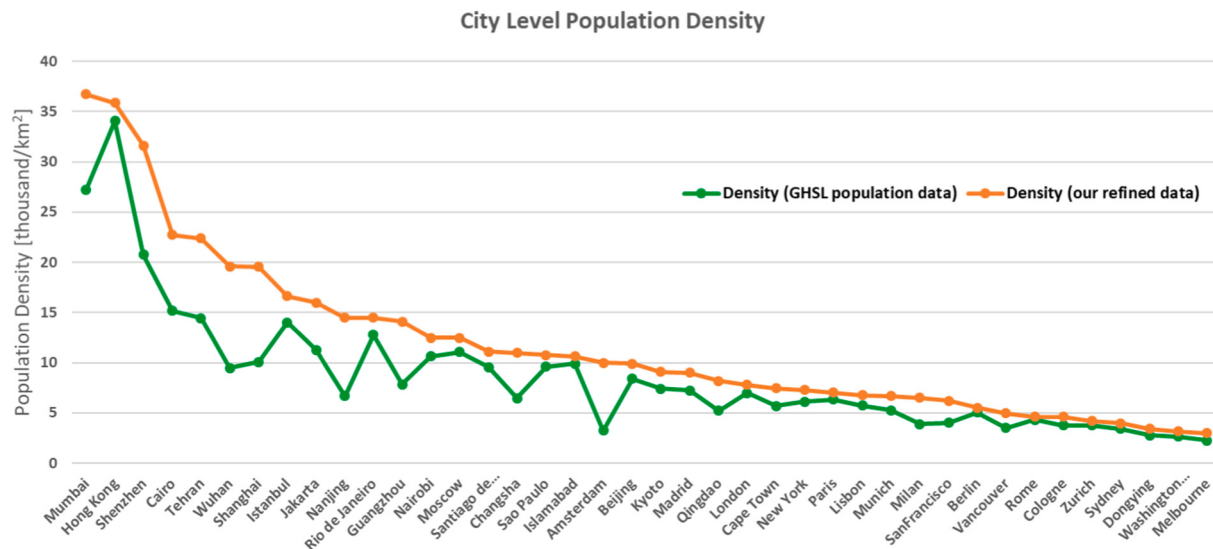


Fig. 7. The per-city population density chart. The densities in green are calculated from the original GHSL population data. The densities in orange are calculated from the refined population data whose spatial distribution at the intra-urban scale is improved. (For interpretation of the references to colour in this figure legend, the reader is referred to the web version of this article.)

Table 1

The distribution of cities in the Global North and the Global South in terms of land area, population, and population density.

		First half in ranking	Second half in ranking
Land area	Global	9	10
	North		
Population	Global South	11	10
	Global	5	14
Population density	North		
	Global South	15	6
Population density	Global	2	17
	North		
Population density	Global South	18	3

natural morphology by human activity are here operationalized by our indicator population density in quantitative manner. We perform the analysis at two scales, the city and the intra-urban scale.

3.2.1. City scale land consumption

At the city scale, we evaluate and compare population densities as proxy for land consumption. In Fig. 7, we compare the population densities of cities that are calculated from GHS-POP data with our refined population data, respectively. As GHS-POP data is produced based on a built-up layer that do not differ industrial and non-industrial areas, we see the effect that population densities are systematically underestimated by compared to our population refinement. According to the estimation from GHS-POP data, the city Hong Kong has the highest population density among the sample 40 cities. However, after the redistribution of population based on our LCZ classification on intra-urban scale, we find the city Mumbai taking the first place with 36,741 people/km² and Hong Kong slides into the second place with 35,881 people/km².

By our analysis, we generally find the urban land consumption is differing immensely across the globe. At the city scale shown in Fig. 7, Mumbai has a population density of 36,741 people/km² which is twelve times denser than Melbourne (2981 people/km²). Moreover, regarding

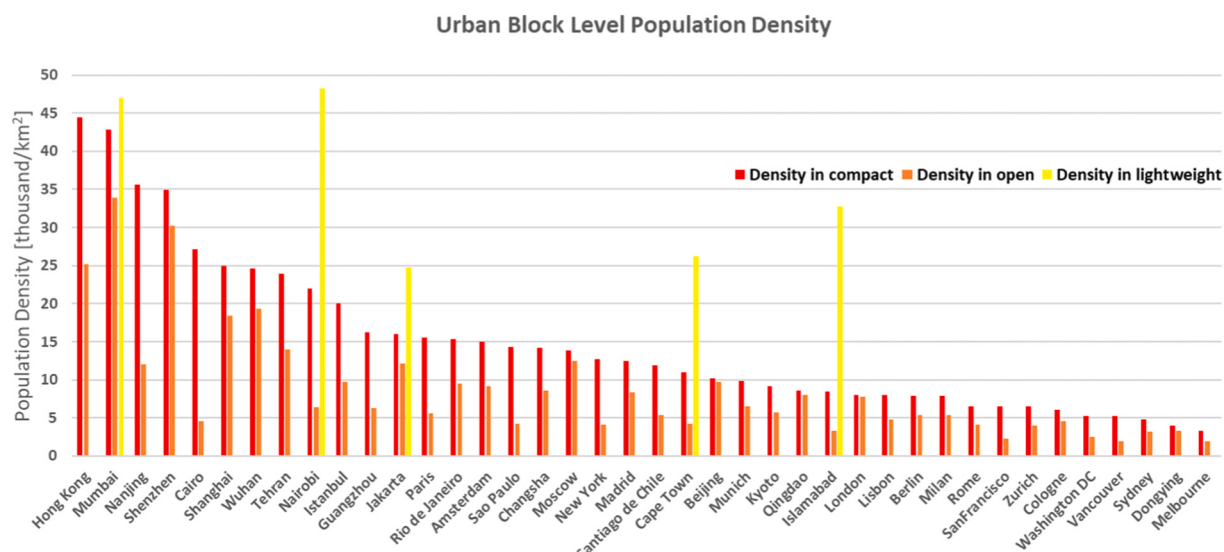


Fig. 8. The population density of intra-urban scale morphological blocks for the 40 cities. These blocks are the compact, the open, and the lightweight blocks.

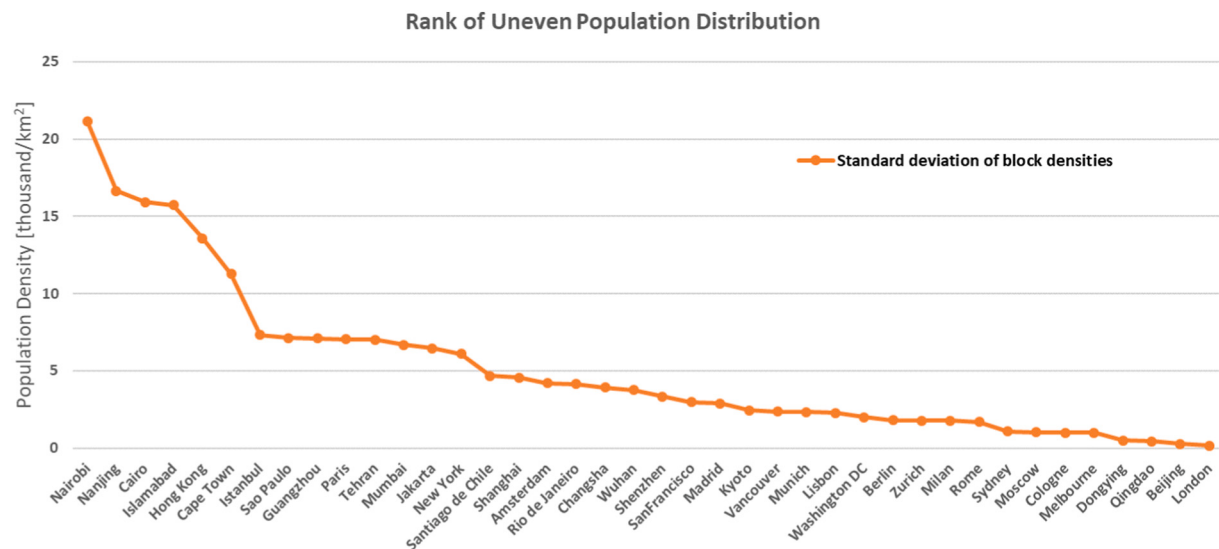


Fig. 9. Unevenness of population distribution within cities indicated by the standard deviation of intra-urban blocks.

the urban land area, we found Hong Kong the second most dense city consuming at the same time the least urban land. In contrary, the city of Melbourne is the least dense city, yet, its urban land area is comparably large, ranking at seventh place. Rankings of urban land areas and population are shown in Fig. 11 and Fig. 12 in Appendix C, respectively.

It is interesting to relate the land consumption data to geographic regions. We conduct a coarse analysis on the correlation between economy and land consumption by dividing the 40 sample cities into two groups: Global North and Global South. Understanding the Global South as geographic regions with a less developed economy (Thérien, 1999), we find 21 cities among our samples belonging to this group and 19 cities to the Global North. We split the rankings of land use, population, and population density into top and bottom halves. For both city groups, the numbers of cities that fall into either half of the three rankings are counted. The results in Table 1 show a specificity for certain geographical regions: 1) cities among our samples in the Global South have larger population than cities in the Global North, 2) cities in the Global South have significantly higher population densities as 18 out of 20 cities in the first half of the population density ranking are Global South cities, and 3) Land use, however, shows no difference across these geographic regions. It can be deduced that better economies show higher per capita land use.

3.2.2. Intra-urban scale land consumption

At the city scale analysis, we found the most dense city, Mumbai, has a population density of 36,741 people/km² (Fig. 7). However, by analyzing on an intra-urban scale, it becomes clear that these mean values on a city-wide scale, cannot represent the local maximum or minimum. As we demonstrate in Fig. 8, we found even higher population densities at intra-urban scale among the sample cities: the lightweight areas of Nairobi and Mumbai, as well as the compact areas of Hong Kong and Mumbai all have population densities larger than 40,000 people/km², significantly denser than the mean values on city scale. Among all areas in the 40 cities, the lightweight class, equivalent to complex, high-density slum structures, of Nairobi are the most dense areas with a population density of 48,241 people/km² (20.73 m² land per person). In this particular example,

Nairobi has at the city scale, a density of a comparatively low number of 12,409 people/km² (80.06 m² land per person) and ranks only the 13th place. The difference between the extreme value and the average in this case is fourfold. We observe these differences for many cities among our sample. This shows impressively that generalized land consumption values at the city level cannot do justice to the complex and spatially highly variable land consumption. We therefore propagate that a spatial differentiation to intra-urban scale is absolutely necessary to use this indicator with high significance.

In addition to the example of Nairobi, in Fig. 8, we also find 17 urban blocks from 12 cities have population densities larger than 20,000 people/km² and up to 48,241 people/km², while 18 urban blocks from 15 cities have population densities smaller than 5000 people/km². The differences are at least four times. These quantitative numbers suggest that urban land consumption is differing significantly across the globe.

We reveal the uneven distribution of land consumption within cities by differentiating the structural LCZs. To do so, we calculate the standard deviations of population densities of the intra-urban morphological blocks as an indicator. As shown in Fig. 9, we reveal Nairobi having the most uneven population distribution among our sample. In contrary, London reveals the highest homogeneity among our samples. Fig. 9 clearly shows that many cities have very uneven population distributions. This supports our argument that an intra-urban resolution is required for a reasonable assessment of urban land consumption.

3.3. Morphological types of cities and population density

3.3.1. Morphological types of cities

Based on our proposed clustering approach, we reveal six morphological types of cities among the 40 sample cities. We identified prominent characteristics for each of the six types, by comparing the cluster centers in Table 2 and inspecting their classification maps. The classification maps of representative cities of each type are illustrated in Fig. 13 in Appendix D. We understand the term “structure” here on an intra-urban block scale, and the term “type” describes the category of

Table 2

This table shows feature values of the six cluster centers. The unit of the numbers is percentage (%).

	Type 1	Type 2	Type 3	Type 4	Type 5	Type 6
Dominating LCZ	Compact	Open	Open-lightweight	Industrial	Lightweight	Compact-open
Share of compact area	63.7	9.3	19.2	13.7	56.1	45.9
Share of open area	8.7	76.9	54.3	39.6	23.6	41.1
Share of lightweight area	0	0	5.0	0	13.3	0
Share of industrial area	27.6	13.8	21.5	46.7	6.9	12.9

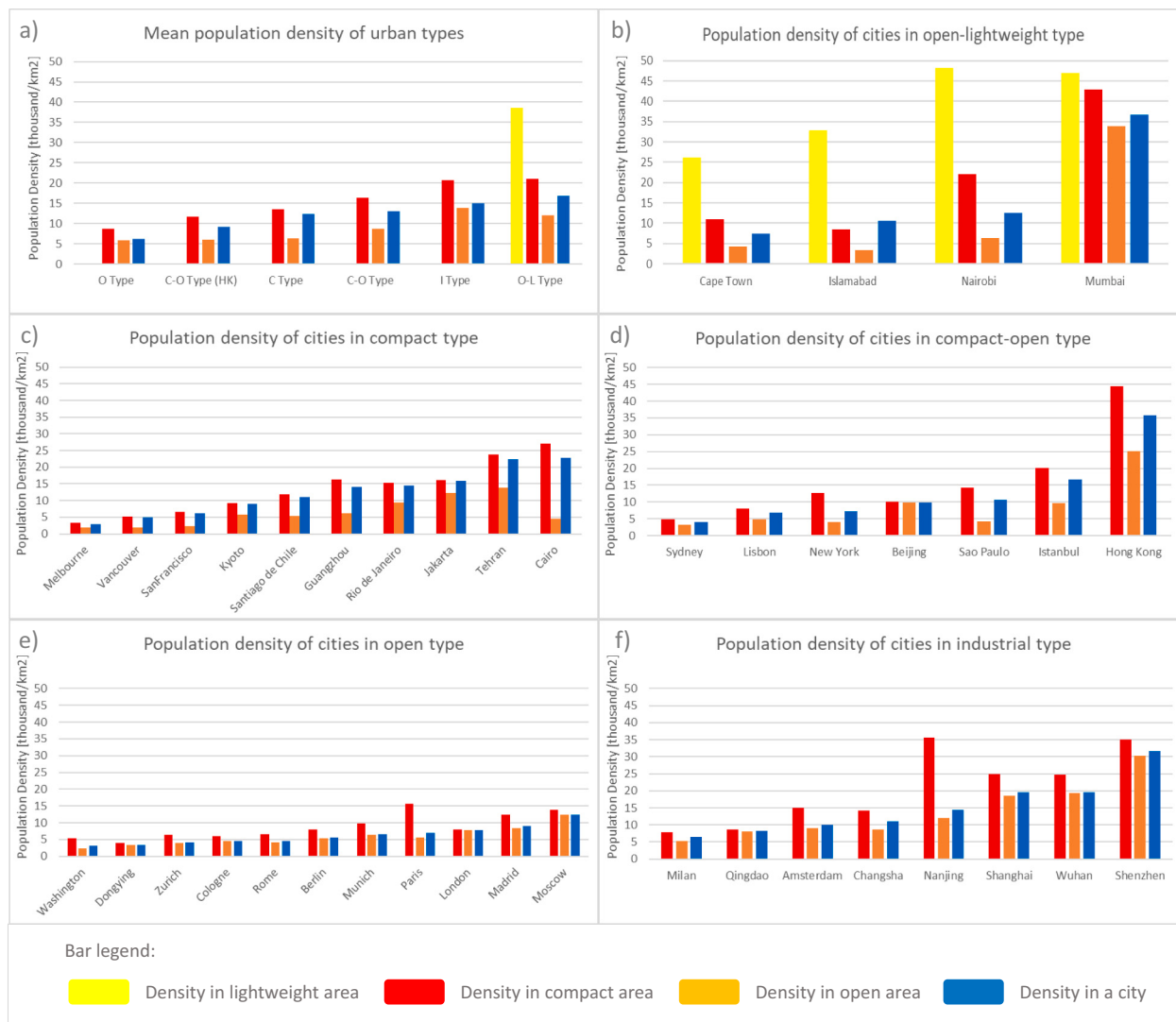


Fig. 10. Population densities of the sample cities organized by the six morphological types. The lightweight type includes only Islamabad so that its density is shown with cities of the open-lightweight type. In a) mean density of city types, O, C—O, C, I, and O-L stand for open, compact-open, compact, industrial, and open-lightweight respectively. C—O type (HK) indicates the mean population density of the compact-open type excluding Hong Kong. The density unit is thousand people per square kilometer. The cities in each subplot are sorted by an increasing order of city scale population density.

urban morphological configurations. For example, a city consists of 64% compact structures, 9% open structures, and 27% industrial structures; The clustering approach classifies this configuration to a *compact type* as in the description of urban morphological formation.

Among our six city types, the *first type* features a group of cities which have predominately compact structures. An average 63.7% of their land have been identified as compact structures. 27.6% of their land are industrial structures. The *second type* groups 11 cities where open structures have a dominant proportion of 76.9%. Nine of the eleven cities are European cities. The *third type* includes the cities of Mumbai, Nairobi, and Cape Town. Their prominent characteristics are 54.3% of open structure and 5% of lightweight structures. The *fourth type* includes eight cities and has an average of 46.7% industrial structures. Six out of the eight cities in this type are from China. The *fifth type* includes only one city, Islamabad. Its specifics are 13.3% are lightweight structures, which is significantly larger than in any other cities among the 40 cities. The *sixth type* is characterized by 45.9% of compact structures and 41.1% of open structures. It is an equal combination of the two structures. To sum up, we have identified six types of urban morphological configurations which are: compact type, open type, open-lightweight type, industrial type, lightweight type, and compact-open type.

3.3.2. Morphological types of cities and population density

In the following, we investigate whether different types of cities, which therefore also have different morphological compositions, feature different types of land consumption. To do so, we analyze the correlation between the clustered morphological types of cities and population densities. We reorganize population densities in terms of the six city types as shown in Fig. 10. Since Islamabad is the only city categorized in the lightweight type, it is analyzed with cities of the open-lightweight type which is the most similar type to it.

For cross type analysis, the mean population density of each urban type is calculated and shown in the subplot a) of Fig. 10. This plot demonstrates a decreasing order of population density from types of open-lightweight, industrial, compact-open, compact, to open. It is interesting in this sequences that the compact type locates between types of open and compact-open. By observing the densities in the compact-open group in subplot d) of Fig. 10, we found that, there is an exceptional sample: Hong Kong. By comparing to Istanbul, the second most dense city in the same type, Hong Kong has a density value twice as large as Istanbul. After excluding Hong Kong, the decreasing order becomes open-lightweight, industrial, compact, compact-open, and open. The order of compact, compact-open, and open basically confirms that

urban structural compactness is positively related to population density.

However, the positive correlation is only valid from the statistical perspective of the mean population densities across types but not for individual cities. For example, Melbourne belongs to the compact type as in subplot **c**) of Fig. 10, but it is the least dense city among the 40 cities. Within the cities of compact type, it appears that the cities of low population density are western cities (Melbourne, Vancouver, and San Francisco). The same situation can also be observed in the compact-open type, as in subplot **d**) of Fig. 10, including Sydney, Lisbon, and New York. For the open type in subplot **e**) of Fig. 10, all cities have a low population density, ten of the eleven cities are western cities (nine from Europe and one from North America). The industrial type rather presents the industrial functionality of cities with an average of 46.7% land as industrial structures. Six of the eight cities are from China. There is no significant evidence for correlation with population density. As shown in subplot **b**) of Fig. 10, the open-lightweight and lightweight types have an outstanding finger print which features a very high population density in the lightweight blocks.

4. Discussion

In this study, we take advantage of the remote sensing data to study urban land consumption at the global scale with an intra-urban spatial resolution. This approach allows the study of land consumption based on a consistent data at a high spatial resolution which allows to picture the spatial variability often lost in aggregated mean values.

Based on our study, we argue that monitoring the global urban land consumption or global urban sustainable development should proceed to an intra-urban resolution. Because our findings refer that per-city wise land consumption indicators have estimated values that severely deviate from the real situation. We also found that urban land consumption is differing significantly across the globe. For example, a citizen living in slum areas of Nairobi has 21 m² lands for living while one could have 530 m² in Melbourne. It is also immensely differing within a city. For example, the population density in lightweight areas of Nairobi is four times denser than the average density of the city. Moreover, we found six types of urban morphological formations among the 40 cities. From a cross type perspective, we reveal a positive correlation between the compactness of urban morphology and population density. We find western cities generally have a lower population density.

In the following we want to critically discuss these main outcomes of our study from various perspectives – conceptual, methodological and geographical:

From a *conceptual aspect*, urban land consumption generally refers to the utilization of land resources due to human activities in cities. Existing studies treat land consumption as modification of natural land to human settlements at city scale (M. Melchiorri et al., 2018, 2019; Taubenböck et al., 2019). Those studies focus on the aspect of urban land usages. Differ from this we associate land consumption to demographical information. And by using the city as well as the intra-urban scale, we unveil a spatially more detailed variability of land consumption, and thus situations of urban inhabitants. We argue the intra-urban scale using morphological descriptions allows to break spatial limitation of administrative boundaries. The aggregated population density analyses inherited from official population data are thus improved. However, there still exist limitations in this domain: Due to the functional information in LCZs, urban inhabitants were not distributed to industrial areas, the redistribution of population is still limited due to the definition of our classification scheme to three aggregated urban morphological residential areas: compact, open, and lightweight structures. It is in our argumentation indeed a more realistic picture of the city, but neither absolutely correct nor spatially or thematically detailed enough. There are still buildings in these three structures that are not constructed for the residential purpose. Accurate mapping of residential buildings / areas is still a major challenge for remote sensing technology. Extra data sources from other fields are complimentary to remote sensing data (Häberle et al., 2019; Hoffmann et al., 2019; R. Huang et al., 2018).

which may allow improved geoinformation in the future. The second limitation is the estimation of living spaces. Due to the missing height information in our baseline remote sensing data the available living spaces remain only indirectly assessed by our LCZ classification scheme. Such detailed information requires an advanced accurate three-dimensional classification. Currently, three-dimensional classification of cities across the globe is restricted by limited access to accurate and consistent global data of height information. Even with these limitations, we believe this study still reveals new knowledge about the land consumption status of our sampled 40 cities at the intra-urban scale.

From a *methodological aspect*, of course, the classification inaccuracies involve limitations. As shown in Fig. 5, the classification accuracy of Mumbai ranges from 59.4% to 72.2%. This is not perfect for the purpose of our applications and the effects for the land consumption analysis remain unknown. It needs to be pointed out that this accuracy is an outcome of a strict evaluation strategy revealing an authentic performance of an algorithm. Although its accuracy is not perfect, currently, its performance is still the state-of-the-art for large area or global applications. With respect to our application, this means any mis-classification will lead to a questionable population redistribution. In general, however, we find our reached accuracy sufficient and the plausibility of our results confirm this. As a second limitation we refer to the difficulty of model transfer of the classification module. There are two classification strategies for our classification task. The first is to train a model on the reference data of the 40 cities, and produce a classification map for any city in the world with this model. The advantage is that one can produce maps for many cities, but the drawback is that the accuracy of those maps is low. The second strategy is to train models on the reference data and only produce maps for these 40 cities. The advantage is the accuracy of these 40 maps is high, but the number of cities is limited. Although some studies (Demuzere et al., 2019; Tong et al., 2020; Yokoya et al., 2017; Zheng et al., 2020) attempt to improve the accuracy of the first strategy, the second strategy is still significantly more accurate than the first strategy. In the context of considering the trade-off in the two strategies, we choose the accurate solution. Thus, our global sample of 40 cities allows a more accurate but possibly not fully comprehensive view on land consumption.

From a geographical point of view, we find a huge difference in urban land consumption across the globe. From 45,000 people/km² in some lightweight areas of cities in the Global South to only 1800 people/km² in some cities of the Global North. The limitation is that we cannot provide quantitative accuracy measures for these numbers as reference data on this spatial level are nonexistent. However, these numbers seem to be very plausible. In any case, we see that the land consumption is highly variable across cities and geographic regions. Therefore, this analysis allows to reflect on urban land consumption. It might support the analysis of the efficiency of land use with respect to other domains.

5. Conclusion and outlook

In this work, we have developed a classification system that fuses Sentinel-1 and Sentinel-2 data using a state-of-the-art semi-supervised technique and produces LCZ classification maps by a topological enhanced ensemble classification technique. With the classification system, LCZ maps of 40 cities around the world are produced. The urban morphological information of LCZ maps allowed us to improve the spatial details of a global population data (GHS-POP) for the 40 cities to an intra-urban scale. With the refined data, a new ranking of the population density of the 40 cities is provided which mitigates the underestimation in GHS-POP caused by distributing population over industrial regions. The cross city population density analysis reveals that the urban land consumption differs immensely across the globe. Beyond, an intra-urban scale land consumption analysis is conducted, which reveals information that is missing in a city scale analysis. We found that, for a same city, an urban block scale population density can be four times larger than the city scale population density. The unevenness of population distribution within cities is also analyzed. Nairobi is reported

to be the most unevenly distributed city. Six urban morphological types are identified among the 40 cities. It is found that the compactness of urban morphology has a positive correlation with population density from a cross type perspective. These findings are only possible as we worked on an intra-urban spatial resolution. Therefore, We argue that monitoring the urban land consumption or urban sustainable development at global scale should proceed to an intra-urban resolution.

Overall, this analysis allows to assess the unevenness of land consumption within and across different cities as well as in different regions across the globe. In a world which is constantly and dynamically urbanizing, this work allows to reveal urban land consumption, to support societal development, and to reflect sustainability.

CRediT authorship contribution statement

Jingliang Hu: Conceptualization, Methodology, Software, Validation, Formal analysis, Investigation, Data curation, Writing – original draft, Writing – review & editing, Visualization. **Yuanyuan Wang:** Conceptualization, Data curation, Formal analysis, Writing – review & editing, Supervision. **Hannes Taubenböck:** Conceptualization,

Resources, Formal analysis, Writing – review & editing. **Xiao Xiang Zhu:** Conceptualization, Supervision, Project administration, Funding acquisition.

Declaration of competing interests

The authors declare that they have no known competing financial interests or personal relationships that could have appeared to influence the work reported in this paper.

Acknowledgments

The work is jointly supported by the European Research Council (ERC) under the European Union's Horizon 2020 - Research and Innovation Framework Programme (grant agreement No. [ERC-2016-StG-714087], Acronym: So2Sat), by the Helmholtz Association through the Framework of Helmholtz AI - Local Unit "Munich Unit @Aeronautics, Space and Transport (MASTR)" and Helmholtz Excellent Professorship "Data Science in Earth Observation - Big Data Fusion for Urban Research".

Appendix A. Sentinel-1 data processing

The Sentinel-1 dual-Pol SAR data used in this paper is prepared by using the ESA SNAP toolbox. The detailed procedure is listed as follows:

- Apply Orbit Profile: A latest released orbit metadata will be downloaded which includes accurate satellite position and velocity information. It leads to a precisely geocoded product.
- Radiometric Calibration: A radar backscatter of the scene surface is achieved from a digital number of the pixel. It reveals a quantitative measure of the surface.
- TOPSAR Deburst: A complete single look complex image is achieved by combining bursts and swaths.
- Polarimetric Speckle Reduction: A speckle-free dual-Pol SAR data is achieved by using the SNAP-integrated refined Lee filter.
- Terrain Correction: A analysis-ready data is achieved which has a ground sampling distance of 10 m and is geocoded in the WGS84/UTM coordinate system. The topographical variation is eliminated with the help of the SRTM.

Appendix B. Semi-supervised data fusion

In this section, mathematical details of the semi-supervised data fusion algorithm are introduced. To precisely explain the algorithm, the terminology has to be defined. Let \mathbf{X}_i represents the Sentinel-1 (\mathbf{X}_1) and Sentinel-2 data (\mathbf{X}_2). $\mathbf{X}_i = [x_i^1, \dots, x_i^p, \dots, x_i^n] \in \mathbb{R}^{m_i \times n_i}$, where p indicates the p^{th} instance ($p \in \{1, 2, 3, \dots, n_i\}$), n is the number of data instances, and m is the dimension of data. Let $\mathbf{X}_i^a \in \mathbb{R}^{m_i \times n_i^a}$ represents the annotated subset of \mathbf{X}_i and $\mathbf{X}_i^{\bar{a}} \in \mathbb{R}^{m_i \times n_i^{\bar{a}}}$ represents the subset without annotation, so that $\mathbf{X}_i^a \cup \mathbf{X}_i^{\bar{a}} = \mathbf{X}_i$, $\mathbf{X}_i^a \cap \mathbf{X}_i^{\bar{a}} = \emptyset$, and $n_i^a + n_i^{\bar{a}} = n_i$. Let the label of instance $x_i^{a,p}$ indicated by $y_i^{a,p}$, thus, the annotated data set is $\{\mathbf{X}_i^a, \mathbf{Y}_i^a\}$, where $\mathbf{Y}_i^a \in \mathbb{R}^{1 \times n_i^a}$.

The semi-supervised fusion algorithm aims to map Sentinel-1 and Sentinel-2 data into a latent space where (1) the data of the same class locate close to each other, and (2) the topological structure of individual data source is preserved. In order to find the latent space, two mathematical terms have to be defined. Firstly, a $(n_1 + n_2)$ by $(n_1 + n_2)$ similarity matrix \mathbf{S} aims to present whether two data instances belong to the same class or not.

$$\mathbf{S} = \begin{pmatrix} \mathbf{S}_{1,1} & \mathbf{S}_{1,2} \\ \mathbf{S}_{2,1} & \mathbf{S}_{2,2} \end{pmatrix} \quad (4)$$

where $\mathbf{S}_{i,j}^{p,q} = 1$, if x_i^p , the p^{th} instances of data \mathbf{X}_i , and x_j^q , the q^{th} instances of data \mathbf{X}_j , belong to the same class, otherwise, $\mathbf{S}_{i,j}^{p,q} = 0$.

The second term, \mathbf{T} , is also a $(n_1 + n_2)$ by $(n_1 + n_2)$ binary matrix, but presents the topological structures of the two data sources.

$$\mathbf{T} = \begin{pmatrix} \mathbf{T}_{1,1} & \mathbf{0} \\ \mathbf{0} & \mathbf{T}_{2,2} \end{pmatrix} \quad (5)$$

where $\mathbf{T}_{1,1}$ and $\mathbf{T}_{2,2}$ represent the topological structures of Sentinel-1 and Sentinel-2 data, respectively. If x_i^p and x_j^q are topologically connected, $t_{i,j}^{p,q} = 1$, otherwise, $t_{i,j}^{p,q} = 0$. The topological structure is the implementation of the semi-supervision concept. It builds up the connections between data of with and without annotations via topology closeness. Conventionally, the topology closeness is practically calculated by k-nearest-neighbor (Liao et al., 2015; Tuia et al., 2014; C. Wang & Mahadevan, 2009). In this work, we applied a recent topological data analysis tool to derive the topology closeness, which has been proven to outperform the k-nearest-neighbor (J. Hu, Hong, Wang, et al., 2019). For more details, please refers to (J. Hu, Hong, Zhu, et al., 2019; L. Li et al., 2015; Singh et al., 2007).

Let \mathbf{f}_1^T and \mathbf{f}_2^T stand for the two projections that respectively bridge Sentinel-1 and Sentinel-2 data to the latent space. Therefore, minimizing the cost function (6) pursues the property (I).

$$\mathcal{C}_s = \sum_{i=1}^2 \sum_{j=1}^2 \sum_{p=1}^{n_1} \sum_{q=1}^{n_2} \| \mathbf{f}_i^T x_i^p - \mathbf{f}_j^T x_j^q \|^2 \mathbf{S}^{i,j}(p, q) \quad (6)$$

Minimizing the cost function (7) preserves the topological structures of the two data sources.

$$\mathcal{C}_t = \sum_{i=1}^2 \sum_{p=1}^{n_1} \sum_{q=1}^{n_2} \| \mathbf{f}_i^T \mathbf{x}_i^p - \mathbf{f}_i^T \mathbf{x}_i^q \|^2 \mathbf{T}^{i,i}(p, q) \quad (7)$$

To minimize the two cost functions simultaneously, it is equal to minimize $\mathcal{L} = \mathcal{C}_s + \mathcal{C}_t$, which turns into an optimization problem $\min_{\mathbf{f}_1, \mathbf{f}_2} \mathcal{L}$. Therefore, the solution to the optimization problem is the smallest non-zero eigenvectors of the generalized eigenvalue decomposition of (8).

$$\tilde{\mathbf{X}}(\mathbf{L}_s + \mathbf{L}_t)\tilde{\mathbf{X}}^T \mathbf{f} = \lambda \tilde{\mathbf{X}}(\mathbf{D}_s + \mathbf{D}_t)\tilde{\mathbf{X}}^T \mathbf{f}, \quad (8)$$

where $\tilde{\mathbf{X}} = \begin{pmatrix} \mathbf{X}_1 & 0 \\ 0 & \mathbf{X}_2 \end{pmatrix}$, \mathbf{D} and \mathbf{L} are the degree matrix and the Laplacian matrix, respectively. After achieving the projections \mathbf{f}_1 and \mathbf{f}_2 , the Sentinel-1 and Sentinel-2 data are mapped into the latent space and are ready for the classification.

Appendix C. Ranks of land area and population

[Fig. 11](#) and [Fig. 12](#) show the ranking of the 40 cities in terms of land area and population, respectively. The values are calculated based on the refined GHS-POP data.

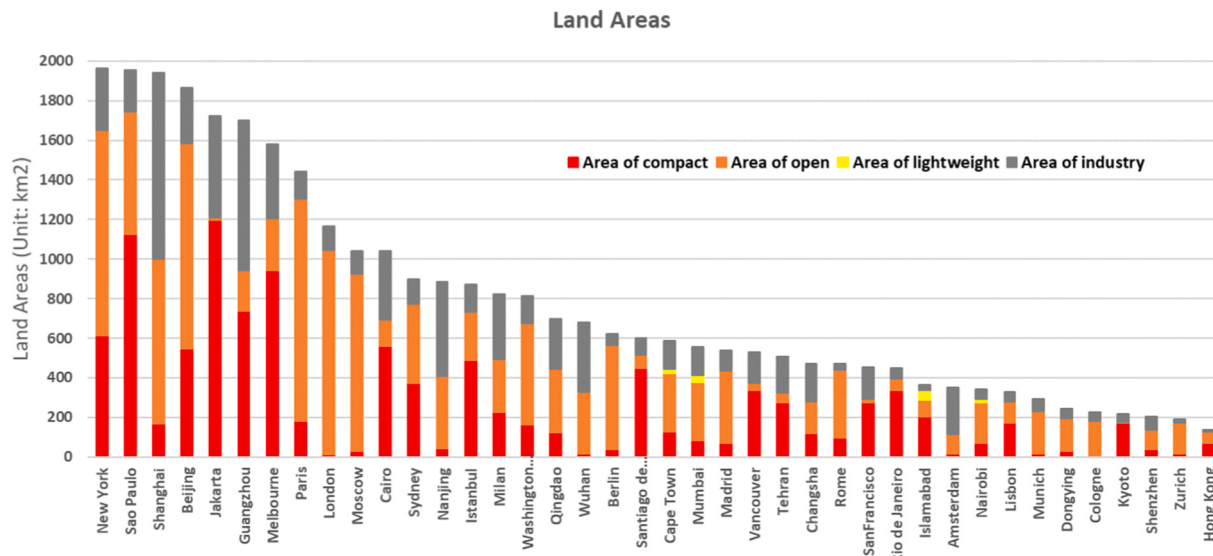


[Fig. 11](#). This figure shows the rank of the 40 cities in terms of land areas. The land areas are the built-up regions that fall into the MUA city extent and are divided by four morphological types, compact, open, lightweight, and industrial structures.

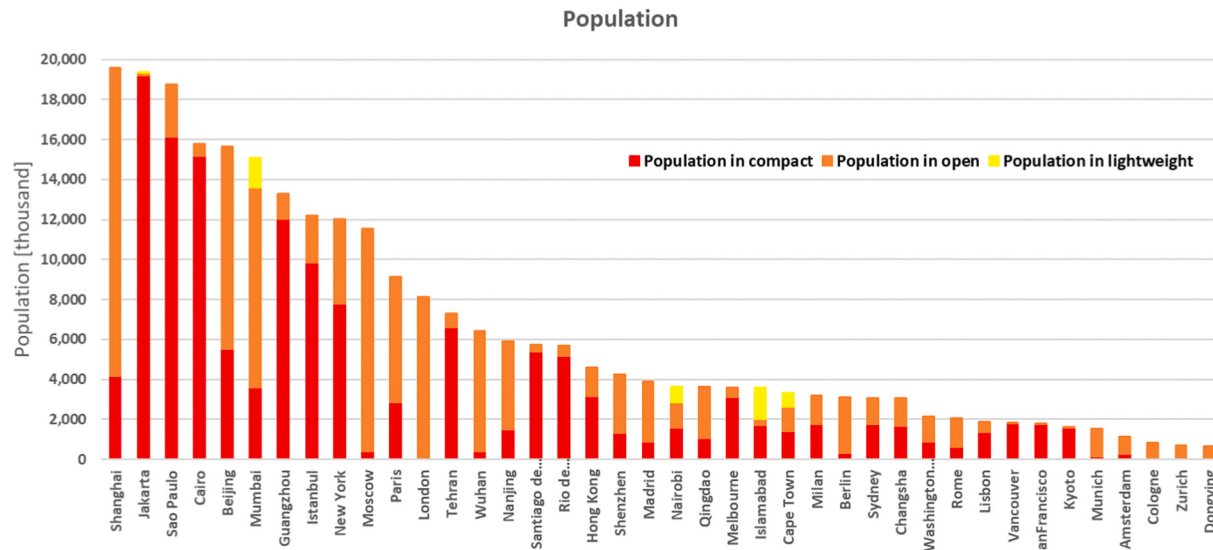


[Fig. 12](#). This figure shows the rank of the 40 cities in terms of population. The total population is given by the GHS-POP data that is spatially overlapped with the MUA urban extent. The population of possible residing urban blocks are also given, which are compact, open, and lightweight structures. The population is calculated after the refinement.

Appendix D. Examples of urban types

Fig. D presents the LCZ maps of representative cities of each urban type. The morphological structures can be visually inspected.

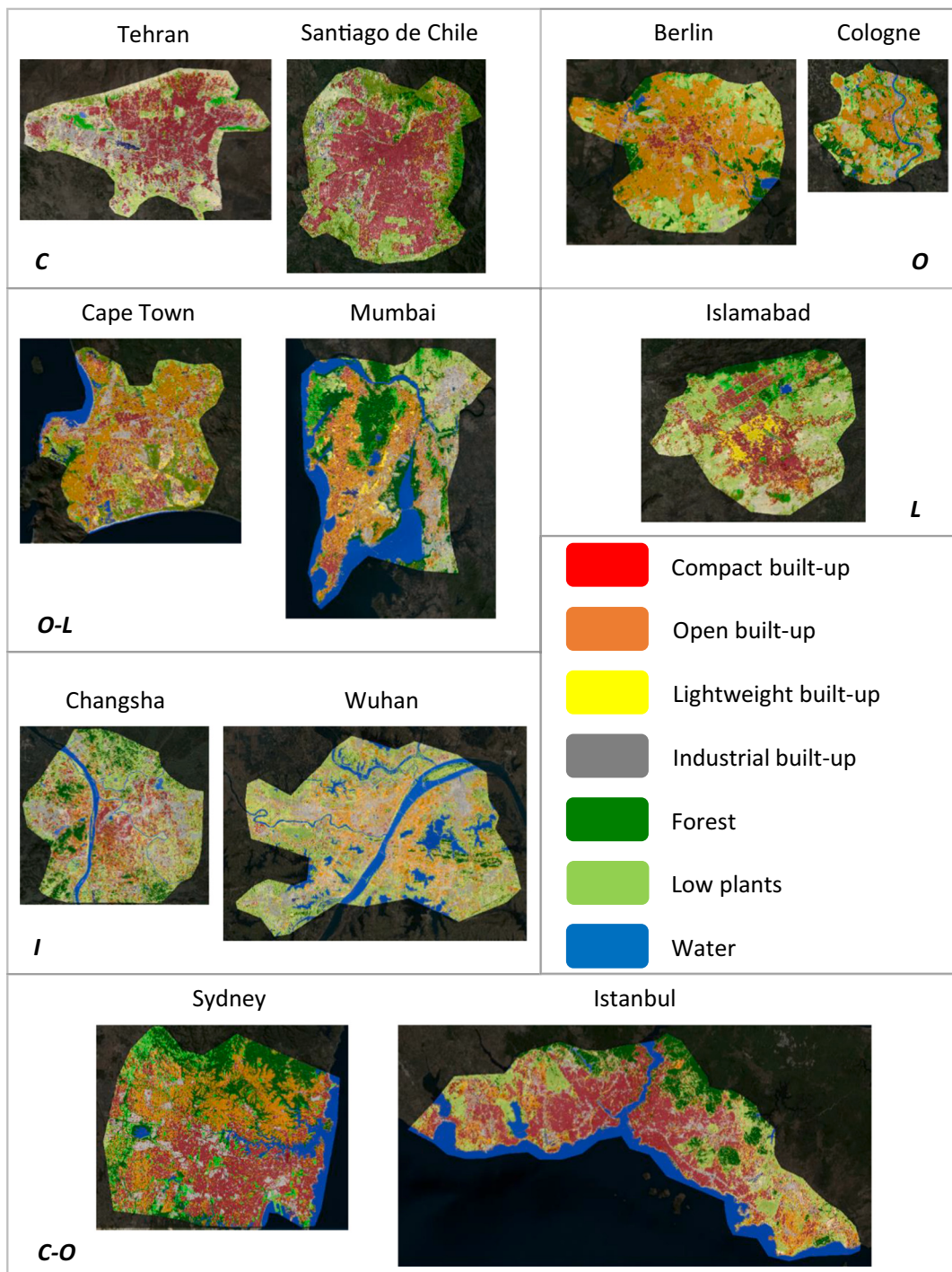


Fig. 13. Classification maps of representative cities for each urban morphological types. All cities are shown under the same map scale. The C, C—O, O, O-L, I, and L stands for compact, open-compact, open, open-lightweight, industrial, and lightweight types.

References

- Arthur, D. and Vassilvitskii, S. 2007. k-means++: The advantages of careful seeding. In *Proceedings of the eighteenth annual ACM-SIAM symposium on Discrete algorithms*, pages 1027–1035. Society for Industrial and Applied Mathematics.
- Ban, Y., Jacob, A., & Gamba, P. (2015). Spaceborne sar data for global urban mapping at 30 m resolution using a robust urban extractor. *ISPRS Journal of Photogrammetry and Remote Sensing*, 103, 28–37.
- Bechtel, B. 2011. Multitemporal landsat data for urban heat island assessment and classification of local climate zones. In *Urban Remote Sensing Event (JURSE), 2011 Joint*, pages 129–132. IEEE.
- Bechtel, B., Alexander, P., Böhner, J., Ching, J., Conrad, O., Feddema, J., Mills, G., See, L., & Stewart, I. (2015). Mapping local climate zones for a worldwide database of the form and function of cities. *ISPRS International Journal of Geo-Information*, 4 (1), 199–219.
- Bechtel, B., & Daneke, C. (2012). Classification of local climate zones based on multiple earth observation data. *IEEE Journal of Selected Topics in Applied Earth Observations and Remote Sensing*, 5(4), 1191–1202.
- Bechtel, B., Pesaresi, M., See, L., Mills, G., Ching, J., Alexander, P., Feddema, J., Florczyk, A., & Stewart, I. (2016). Towards consistent mapping of urban structure-global human settlement layer and local climate zones. *ISPRS-International Archives of the Photogrammetry, Remote Sensing and Spatial Information Sciences*, 41, 1371–1378.
- Bechtel, B., See, L., Mills, G., & Foley, M. (2016). Classification of local climate zones using sar and multispectral data in an arid environment. *IEEE Journal of Selected Topics in Applied Earth Observations and Remote Sensing*, 9(7), 3097–3105.
- Benediktsson, J. A., Pesaresi, M., & Amazon, K. (2003). Classification and feature extraction for remote sensing images from urban areas based on morphological transformations. *IEEE Transactions on Geoscience and Remote Sensing*, 41(9), 1940–1949.
- Bimonte, S., & Stabile, A. (2017). Land consumption and income in Italy: A case of inverted eck. *Ecological Economics*, 131, 36–43.
- Boyce, R. R. (1963). Changing patterns of urban land consumption. *The Professional Geographer*, 15(2), 19–24.
- Breiman, L. (2001). Random forests. *Machine Learning*, 45(1), 5–32.
- Chazal, F., Guibas, L. J., Oudot, S. Y., & Skraba, P. (2013). Persistence-based clustering in riemannian manifolds. *Journal of the ACM (JACM)*, 60(6), 41.
- Comaniciu, D., & Meer, P. (2002). Mean shift: A robust approach toward feature space analysis. *IEEE Transactions on Pattern Analysis & Machine Intelligence*, 5, 603–619.
- d'Amour, C. B., Reitsma, F., Baiocchi, G., Barthel, S., Güneralp, B., Erb, K.-H., ... Seto, K. C. (2017). Future urban land expansion and implications for global croplands. *Proceedings of the National Academy of Sciences*, 114(34), 8939–8944.
- Danylo, O., See, L., Bechtel, B., Schepaschenko, D., & Fritz, S. (2016). Contributing to wudapt: A local climate zone classification of two cities in Ukraine. *IEEE Journal of Selected Topics in Applied Earth Observations and Remote Sensing*, 9(5), 1841–1853.
- Demuzere, M., Bechtel, B., & Mills, G. (2019). Global transferability of local climate zone models. *Urban Climate*, 27, 46–63.
- Doxsey-Whitfield, E., MacManus, K., Adamo, S. B., Pistoletti, L., Squires, J., Borkovska, O., & Baptista, S. R. (2015). Taking advantage of the improved availability of census data: A first look at the gridded population of the world, version 4. *Papers in Applied Geography*, 1(3), 226–234.
- Elghazel, H., Aussem, A., and Perraud, F. 2011. Trading-off diversity and accuracy for optimal ensemble tree selection in random forests. In *Ensembles in Machine Learning Applications*, pages 169–179. Springer.
- Esch, T., Heldens, W., Hirner, A., Keil, M., Marconcini, M., Roth, A., Zeidler, J., Dech, S., & Strano, E. (2017). Breaking new ground in mapping human settlements from space—the global urban footprint. *ISPRS Journal of Photogrammetry and Remote Sensing*, 134, 30–42.
- Ester, M., Kriegel, H.-P., Sander, J., Xu, X., et al. (1996). A density-based algorithm for discovering clusters in large spatial databases with noise. In *Kdd, volume*, 96, 226–231.
- Fauvel, M., Benediktsson, J. A., Chanussot, J., & Sveinsson, J. R. (2008). Spectral and spatial classification of hyperspectral data using svms and morphological profiles. *IEEE Transactions on Geoscience and Remote Sensing*, 46(11), 3804–3814.
- Freire, S., MacManus, K., Pesaresi, M., Doxsey-Whitfield, E., & Mills, J. (2016). Development of new open and free multi-temporal global population grids at 250 m resolution.
- Frigui, H., & Krishnapuram, R. (1997). Clustering by competitive agglomeration. *Pattern Recognition*, 30(7), 1109–1119.
- Gál, T., Bechtel, B., & Unger, J. (2015). Comparison of two different local climate zone mapping methods.
- Geletić, J., & Lehnhert, M. (2016). Gis-based delineation of local climate zones: The case of medium-sized central european cities. *Moravian Geographical Reports*, 24(3), 2–12.
- Gerundo, R., & Grimaldi, M. (2011). The measure of land consumption caused by urban planning. *Procedia Engineering*, 21, 1152–1160.
- Glaeser, E. (2011). *Triumph of the city: How urban spaces make us human* (Pan Macmillan).
- Gorelick, N., Hancher, M., Dixon, M., Ilyushchenko, S., Thau, D., & Moore, R. (2017). Google earth engine: Planetary-scale geospatial analysis for everyone. *Remote Sensing of Environment*, 202, 18–27.
- Grekousis, G., & Mountrakis, G. (2015). Sustainable development under population pressure: Lessons from developed land consumption in the conterminous us. *PLoS One*, 10(3), Article e0119675.
- Häberle, M., Werner, M., and Zhu, X. X. 2019. Building type classification from social media texts via geo-spatial textmining. In *IGARSS 2019-2019 IEEE International Geoscience and Remote Sensing Symposium*, pages 10047–10050. IEEE.
- Hänsch, R., Ley, A., and Hellwich, O. 2017. Correct and still wrong: The relationship between sampling strategies and the estimation of the generalization error. In *2017 IEEE International Geoscience and Remote Sensing Symposium (IGARSS)*, pages 3672–3675. IEEE.
- He, B.-J., Zhao, Z.-Q., Shen, L.-D., Wang, H.-B., & Li, L.-G. (2019). An approach to examining performances of cool/hot sources in mitigating/enhancing land surface temperature under different temperature backgrounds based on landsat 8 image. *Sustainable Cities and Society*, 44, 416–427.
- Hoffmann, E. J., Wang, Y., Werner, M., Kang, J., & Zhu, X. X. (2019). Model fusion for building type classification from aerial and street view images. *Remote Sensing*, 11 (11), 1259.
- Hu, J., Ghamisi, P., & Zhu, X. X. (2018). Feature extraction and selection of sentinel-1 dual-pol data for global-scale local climate zone classification. *ISPRS International Journal of Geo-Information*, 7(9), 379.
- Hu, J., Hong, D., Wang, Y., & Zhu, X. X. (2019). A comparative review of manifold learning techniques for hyperspectral and polarimetric sar image fusion. *Remote Sensing*, 11(6), 681.
- Hu, J., Hong, D., & Zhu, X. X. (2019). Mima: Mapper-induced manifold alignment for semi-supervised fusion of optical image and polarimetric sar data. *IEEE Transactions on Geoscience and Remote Sensing*, 57(11), 9025–9040. ISSN 1558-0644 <https://doi.org/10.1109/TGRS.2019.2924113>.
- Huang, R., Taubenböck, H., Mou, L., and Zhu, X. X. 2018. Classification of settlement types from tweets using lda and lstm. In *IGARSS 2018-2018 IEEE International Geoscience and Remote Sensing Symposium*, pages 6408–6411. IEEE.
- Huang, X., Wang, C., and Li, Z. 2019. High-resolution population grid in the conus using microsoft building footprints: a feasibility study. In *Proceedings of the 3rd ACM SIGSPATIAL International Workshop on Geospatial Humanities*, pages 1–9.
- Jain, A. K., Murty, M. N., & Flynn, P. J. (1999). Data clustering: A review. *ACM computing surveys (CSUR)*, 31(3), 264–323.
- Kaloustian, N., Tamminga, M., & Bechtel, B. (2017). Local climate zones and annual surface thermal response in a mediterranean city. In *2017 Joint Urban Remote Sensing Event (JURSE)* (pp. 1–4). <https://doi.org/10.1109/JURSE.2017.7924597>.
- Kuang, B., Lu, X., Han, J., Fan, X., & Zuo, J. (2020). *How urbanization influence urban land consumption intensity: Evidence from China* (p. 102103). Habitat International.
- Lehnert, M., Geletić, J., Husák, J., & Vysoudil, M. (2015). Urban field classification by “local climate zones” in a medium-sized central european city: The case of Olomouc (Czech Republic). *Theoretical and Applied Climatology*, 122(3–4), 531–541.
- Lelovics, E., Unger, J., Gál, T., & Gál, C. V. (2014). Design of an urban monitoring network based on local climate zone mapping and temperature pattern modelling. *Climate Research*, 60(1), 51–62.
- Li, C., Gong, P., Wang, J., Zhu, Z., Biging, G. S., Yuan, C., , Li, X., et al. (2017). The first all-season sample set for mapping global land cover with landsat-8 data. *Science Bulletin*, 62(7), 508–515.
- Li, L., Cheng, W.-Y., Glicksberg, B. S., Gottesman, O., Tamler, R., Chen, R., Bottinger, E. P., and Dudley, J. T. 2015. Identification of type 2 diabetes subgroups through topological analysis of patient similarity. *Science translational medicine*, 7(311): 311ra174–311ra174.
- Liao, W., Pižurica, A., Bellens, R., Gautama, S., & Philips, W. (2015). Generalized graph-based fusion of hyperspectral and lidar data using morphological features. *IEEE Geoscience and Remote Sensing Letters*, 12(3), 552–556.
- Lisini, G., Salenting, A., Du, P., & Gamba, P. (2017). Sar-based urban extents extraction: From envisat to sentinel-1. *IEEE Journal of Selected Topics in Applied Earth Observations and Remote Sensing*, 11(8), 2683–2691.
- Marconcini, M., Metz-Marconcini, A., Üreyen, S., Palacios-Lopez, D., Hanke, W., Bachofner, F., Zeidler, J., Esch, T., Gorelick, N., Kakarla, A., et al. 2019. Outlining where humans live—the world settlement footprint 2015. *arXiv preprint arXiv: 1910.12707*.
- Martinuzzi, S., Gould, W. A., & Gonzalez, O. M. R. (2007). Land development, land use, and urban sprawl in Puerto Rico integrating remote sensing and population census data. *Landscape and Urban Planning*, 79(3–4), 288–297.
- Melchiorri, M., Florczyk, A., Freire, S., Schiavina, M., Pesaresi, M., & Kemper, T. (2018). Unveiling 25 years of planetary urbanization with remote sensing: Perspectives from the global human settlement layer. *Remote Sensing*, 10(5), 768.
- Melchiorri, M., Pesaresi, M., Florczyk, A. J., Corbane, C., and Kemper, T. 2019. Principles and applications of the global human settlement layer as baseline for the land use efficiency indicator—sdg 11.3. 1. *ISPRS International Journal of Geo-Information*, 8 (2):96.
- Ng, A. Y., Jordan, M. I., & Weiss, Y. (2002). On spectral clustering: Analysis and an algorithm. In *Advances in neural information processing systems*, pages 849–856.
- Nicolau, R., David, J., Caetano, M., & Pereira, J. (2019). Ratio of land consumption rate to population growth rate—Analysis of different formulations applied to mainland Portugal. *ISPRS International Journal of Geo-Information*, 8(1), 10.
- Perera, N., & Emmanuel, R. (2018). A “local climate zone” based approach to urban planning in Colombo, Sri Lanka. *Urban Climate*, 23, 188–203.
- Pesaresi, M., Huadong, G., Blaes, X., Ehrlich, D., Ferri, S., Gueguen, L., , Lu, L., et al. (2013). A global human settlement layer from optical hr/vhr rs data: Concept and first results. *IEEE Journal of Selected Topics in Applied Earth Observations and Remote Sensing*, 6(5), 2102–2131.
- Qiu, C., Mou, L., Schmitt, M., & Zhu, X. X. (2019). LCZ-based urban land cover classification from multi-seasonal Sentinel-2 images with a recurrent residual network. *ISPRS Journal of Photogrammetry and Remote Sensing*, 154, 151–162.
- Rainforth, T., and Wood, F. 2015. Canonical correlation forests. *arXiv preprint arXiv: 1507.05444*.
- Reichstein, M., Camps-Valls, G., Stevens, B., Jung, M., Denzler, J., Carvalhais, N., et al. (2019). Deep learning and process understanding for data-driven earth system science. *Nature*, 566(7743), 195–204.

- Salvati, L., Zambon, I., Chelli, F. M., & Serra, P. (2018). Do spatial patterns of urbanization and land consumption reflect different socioeconomic contexts in europe? *Science of the Total Environment*, 625, 722–730.
- Sapena, M., Wurm, M., Taubenböck, H., Tuia, D., & Ruiz, L. A. (2021). Estimating quality of life dimensions from urban spatial pattern metrics. *Computers, Environment and Urban Systems*, 85, 101549.
- Schiavina, M., Freire, S., and MacManus, K. 2019. Ghs population grid multitemporal (1975, 1990, 2000, 2015). European Commission, Joint Research Centre (JRC) [Dataset] PID: DOI: 10.2905/42E8BE89-54FF-464E-BE7B-BF9E64DA5218 PID: <http://data.europa.eu/89h/0c6b9751-a71f-4062-830b-43c9f432370f>.
- Schmitt, M., Hughes, L. H., Qiu, C., and Zhu, X. X. 2019. Aggregating cloud-free Sentinel-2 images with google earth engine. to appear.
- Singh, G., Mémoli, F., & Carlsson, G. E. (2007). Topological methods for the analysis of high dimensional data sets and 3d object recognition. In *SPBG*, pages, 91–100.
- Stevens, F. R., Gaughan, A. E., Linard, C., & Tatem, A. J. (2015). Disaggregating census data for population mapping using random forests with remotely-sensed and ancillary data. *PLoS One*, 10(2).
- Stewart, I. and Oke, T. 2009. Classifying urban climate field sites by “local climate zones”: The case of Nagano, Japan. In *IN: Seventh International Conference on Urban Climate*, volume 29.
- Stewart, I. D., & Oke, T. R. (2012). Local climate zones for urban temperature studies. *Bulletin of the American Meteorological Society*, 93(12), 1879–1900.
- Stewart, I. D., Oke, T. R., & Krayenhoff, E. S. (2014). Evaluation of the “local climate zone”scheme using temperature observations and model simulations. *International Journal of Climatology*, 34(4), 1062–1080.
- Stokes, E. C., & Seto, K. C. (2016). Climate change and urban land systems: Bridging the gaps between urbanism and land science. *Journal of Land Use Science*, 11(6), 698–708.
- Tatem, A. J. (2017). Worldpop, open data for spatial demography. *Scientific data*, 4(1), 1–4.
- Taubenböck, H., Weigand, M., Esch, T., Staab, J., Wurm, M., Mast, J., & Dech, S. (2019). A new ranking of the world’s largest cities—Do administrative units obscure morphological realities? *Remote Sensing of Environment*, 232, 111353.
- Therien, J.-P. (1999). Beyond the north-south divide: The two tales of world poverty. *Third World Quarterly*, 20(4), 723–742.
- Tong, X.-Y., Xia, G.-S., Lu, Q., Shen, H., Li, S., You, S., & Zhang, L. (2020). Land-cover classification with high-resolution remote sensing images using transferable deep models. *Remote Sensing of Environment*, 237, 111322.
- Tuia, D., Volpi, M., Trolliet, M., & Camps-Valls, G. (2014). Semisupervised manifold alignment of multimodal remote sensing images. *IEEE Transactions on Geoscience and Remote Sensing*, 52(12), 7708–7720.
- United Nations. 2015a. World urbanization prospects: The 2014 revision. <https://population.un.org/wup/Publications/Files/WUP2014-Report.pdf>. Accessed: 2019-08-09.
- United Nations. 2015b. Resolution adopted by the general assembly on 25 september 2015. In *Transforming Our World: The 2030 Agenda for Sustainable Development*. United Nations New York, NY. URL https://www.un.org/ga/search/view_doc.asp?symbol=A/RES/70/1&Lang=E.
- United Nations. 2016. The world’s cities in 2016. http://www.un.org/en/development/desa/population/publications/pdf/urbanization/the_worlds_cities_in_2016_data_a_booklet.pdf. Accessed: 2018-04-10.
- United Nations. 2018. The world’s cities in 2018. https://www.un.org/en/events/citiesday/assets/pdf/the_worlds_cities_in_2018_data_booklet.pdf. Accessed: 2019-06-14.
- United Nations Habitat. 2016. Goal 11. make cities and human settlements inclusive, safe, resilient and sustainable. <https://unstats.un.org/sdgs/metadata/?Text=&Goal=&Target=11.3>.
- Von Luxburg, U. (2007). A tutorial on spectral clustering. *Statistics and Computing*, 17(4), 395–416.
- Wang, C. and Mahadevan, S. 2009. A general framework for manifold alignment. In *AAAI fall symposium: manifold learning and its applications*, pages 53–58.
- Wang, S., Cebula, R. J., Liu, X., and Foley, M. 2020. Housing prices and urban land use efficiency. *Applied Economics Letters*, pages 1–4.
- Wang, Y., Huang, C., Feng, Y., Zhao, M., and Gu, J. 2020. Using earth observation for monitoring sdg 11.3. 1-ratio of land consumption rate to population growth rate in mainland China. *Remote Sensing*, 12(3):357.
- Xu, L., Wang, X., Liu, J., He, Y., Tang, J., Nguyen, M., & Cui, S. (2019). Identifying the trade-offs between climate change mitigation and adaptation in urban land use planning: An empirical study in a coastal city. *Environment International*, 133, 105162.
- Xu, Y., Ren, C., Cai, M., Edward, N. Y. Y., & Wu, T. (2017). Classification of local climate zones using aster and landsat data for high-density cities. *IEEE Journal of Selected Topics in Applied Earth Observations and Remote Sensing*, 10(7), 3397–3405.
- Xu, Z., Chen, J., Xia, J., Du, P., Zheng, H., & Gan, L. (2018). Multisource earth observation data for land-cover classification using random forest. *IEEE Geoscience and Remote Sensing Letters*, 15(5), 789–793.
- Yang, J., Jin, S., Xiao, X., Jin, C., Xia, J. C., Li, X., & Wang, S. (2019). Local climate zone ventilation and urban land surface temperatures: Towards a performance-based and wind-sensitive planning proposal in megacities. *Sustainable Cities and Society*, 47, 101487.
- Yang, J., Sun, J., Ge, Q., & Li, X. (2017). Assessing the impacts of urbanization-associated green space on urban land surface temperature: A case study of Dalian, China. *Urban Forestry & Urban Greening*, 22, 1–10.
- Yang, J., Wang, Y., Xiu, C., Xiao, X., Xia, J., & Jin, C. (2020). Optimizing local climate zones to mitigate urban heat island effect in human settlements. *Journal of Cleaner Production*, 275, 123767.
- Yang, J., Zhan, Y., Xiao, X., Xia, J. C., Sun, W., & Li, X. (2020). Investigating the diversity of land surface temperature characteristics in different scale cities based on local climate zones. *Urban Climate*, 34, 100700.
- Yokoya, N., Ghamisi, P., and Xia, J. 2017. Multimodal, multitemporal, and multisource global data fusion for local climate zones classification based on ensemble learning. In *Geoscience and Remote Sensing Symposium (IGARSS), 2017 IEEE International*, pages 1197–1200. IEEE.
- Zelnik-Manor, L., & Perona, P. (2005). Self-tuning spectral clustering. In *Advances in neural information processing systems*, pages, 1601–1608.
- Zhang, Y., Zhang, H., & Lin, H. (2014). Improving the impervious surface estimation with combined use of optical and Sar remote sensing images. *Remote Sensing of Environment*, 141, 155–167.
- Zheng, Z., Wang, J., Shan, B., He, Y., Liao, C., Gao, Y., & Yang, S. (2020). A new model for transfer learning-based mapping of burn severity. *Remote Sensing*, 12(4), 708.
- Zhu, X. X., Hu, J., Qiu, C., Shi, Y., Kang, J., Mou, L., ... Wang, Y. (2020). So2sat lcz42: A benchmark data set for the classification of global local climate zones [software and data sets]. *IEEE Geoscience and Remote Sensing Magazine*, 8(3), 76–89. <https://doi.org/10.1109/MGRS.2020.2964708>.
- Zhu, X. X., Tuia, D., Mou, L., Xia, G.-S., Zhang, L., Xu, F., & Fraundorfer, F. (2017). Deep learning in remote sensing: A comprehensive review and list of resources. *IEEE Geoscience and Remote Sensing Magazine*, 5(4), 8–36.
- Zhu, Z., Woodcock, C. E., Rogan, J., & Kellndorfer, J. (2012). Assessment of spectral, polarimetric, temporal, and spatial dimensions for urban and peri-urban land cover classification using landsat and sar data. *Remote Sensing of Environment*, 117, 72–82.